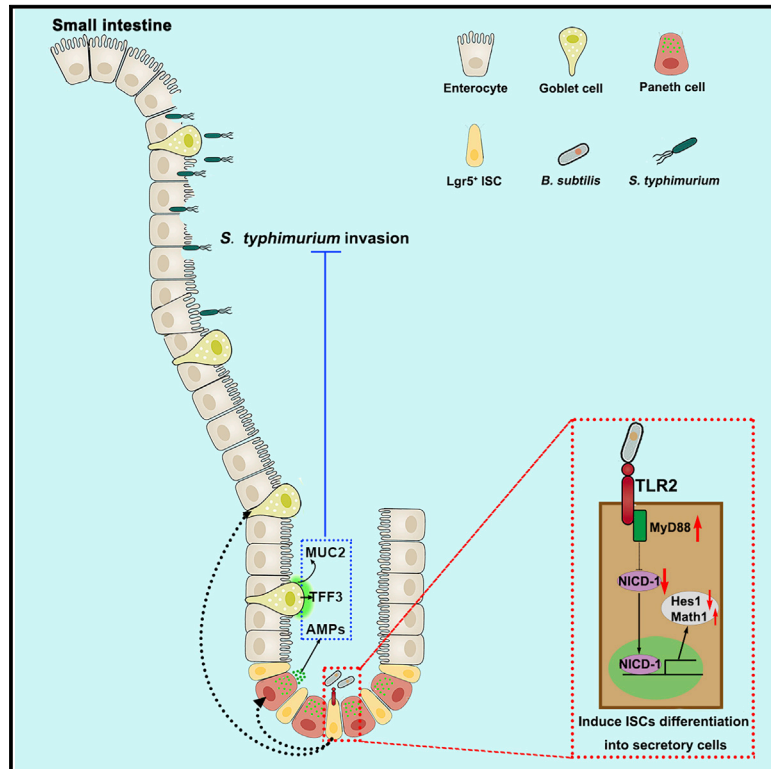


Bacillus subtilis programs the differentiation of intestinal secretory lineages to inhibit *Salmonella* infection

Graphical abstract



Authors

Qihang Hou, Junpeng Jia, Jian Lin, Linda Zhu, Shuang Xie, Qinghua Yu, Yuchen Li

Correspondence

qinghua.yu@diprobio.com (Q.Y.), yuchengli@njau.edu.cn (Y.L.)

In brief

Hou et al. establish various bacteria and intestinal organoid co-culture systems and demonstrate that *B. subtilis* inhibits Notch pathway signaling in an LTA-TLR2-dependent manner, programs intestinal epithelial cells to differentiate toward a secretory cell fate, and increases production of mucins and antimicrobial peptides to defend against *S. typhimurium* infection.

Highlights

- Bacteria and intestinal organoid co-culture system is established
- *B. subtilis* programs the differentiation of intestinal secretory lineages
- *B. subtilis* inhibits Notch pathway signaling in an LTA-TLR2-dependent manner
- *B. subtilis* increases the production of AMPs to defend against *S. typhimurium* infection



Article

Bacillus subtilis programs the differentiation of intestinal secretory lineages to inhibit *Salmonella* infection

Qihang Hou,^{1,3,4} Junpeng Jia,^{1,4} Jian Lin,¹ Linda Zhu,¹ Shuang Xie,¹ Qinghua Yu,^{1,2,*} and Yuchen Li^{1,5,*}¹MOE Joint International Research Laboratory of Animal Health and Food Safety, College of Veterinary Medicine, Nanjing Agricultural University, Weigang 1, Nanjing, Jiangsu 210095, P.R. China²Laboratory of Microbiology, Immunology and Metabolism, Diprobio (Shanghai) Co., Ltd., Shanghai 200335, P.R. China³State Key Laboratory of Animal Nutrition, College of Animal Science and Technology, China Agricultural University, Haidian District, Beijing 100193, P.R. China⁴These authors contributed equally⁵Lead contact*Correspondence: qinghua.yu@diprobio.com (Q.Y.), yuchengli@njau.edu.cn (Y.L.)<https://doi.org/10.1016/j.celrep.2022.111416>

SUMMARY

The role of intestinal microbiota on fate determination of intestinal epithelial cells has not been extensively examined. In this study, we explore the effect of *Bacillus subtilis* on programmed intestinal epithelial differentiation. We find that *B. subtilis* stimulates the differentiation of intestinal secretory cells. Moreover, *B. subtilis* inhibits the Notch pathway to reduce the expression of hairy and enhancer of split 1, thereby shifting intestinal stem cell differentiation toward a secretory cell fate. Moreover, we demonstrate that the programming effect of *B. subtilis* on intestinal differentiation is Toll-like receptor 2 pathway dependent. *B. subtilis* is associated with increased numbers of Paneth and goblet cells in the intestine. This results in the production of antimicrobial peptides to protect the intestinal mucosal barrier against *Salmonella typhimurium*. This study demonstrates that *B. subtilis* contributes to the differentiation of secretory cells by affecting Notch pathway signaling to maintain the intestinal barrier.

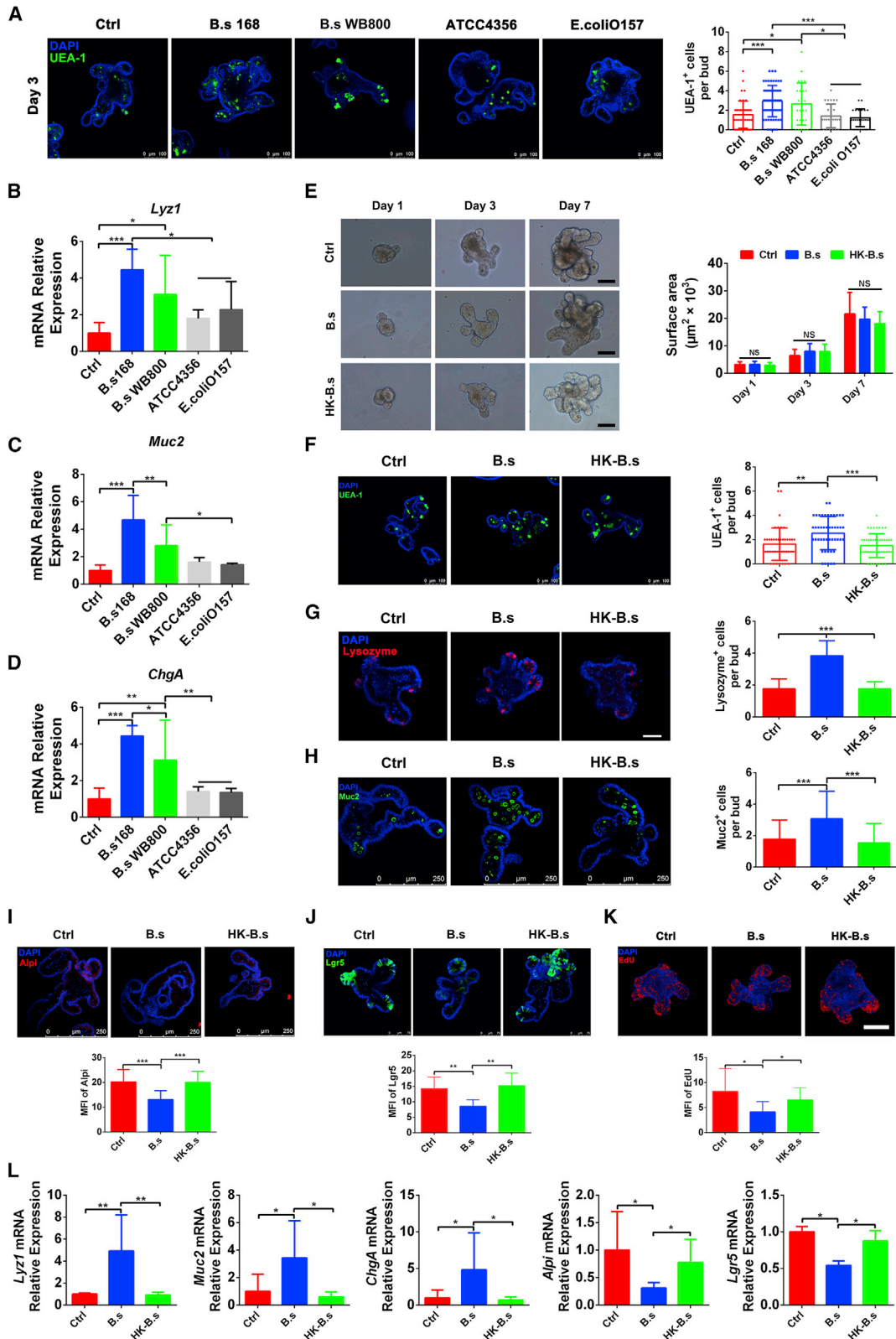
INTRODUCTION

Host-associated microbiota play critical roles in animal health and development (Kundu et al., 2017); the mechanisms by which they influence processes, such as cell differentiation, remain unknown. Understanding the relationship between microbiota and intrinsic developmental pathways is key for developing strategies to promote intestinal homeostasis under pathogen stress. Animal models have been used to investigate many biological questions but are often too complex to directly elucidate the interactions between intestinal microbiota and epithelial cells. Previous studies have shown that intestinal organoid culture systems (Ootani et al., 2009; Sato et al., 2009) can be used in disease modeling, drug development, and *in vitro* examination of cellular differentiation (Kretzschmar and Clevers, 2016). Intestinal stem cell (ISC)-derived organoids contain many types of differentiated epithelial cells and allow for proliferation and differentiation of the intestinal epithelium under specific conditions. Co-culture models of intestinal organoids with different microbiota enable these complicated interactions to be studied *in vitro* (Dutta and Clevers, 2017; In et al., 2016). Organoids therefore have great potential to improve our current understanding of intestinal microbiota-host interactions and to replace or reduce the dependence on animal models in the field.

The intestinal epithelial lining is in continuous contact with the intestinal microbiota and is renewed by ISCs (Hou et al., 2017). ISCs can differentiate into five major cell types in the small intestine but only three in the colon. Primary epithelial cells are known as absorptive enterocytes in the small intestine. Secretory cell lineages, including Paneth cells, support the ISC niche and secrete antimicrobial peptides, mucus-producing goblet cells, various hormone-secreting enteroendocrine cells, M cells, and tuft cells. Notably, the colonic crypts lack Paneth cells but contains Paneth-like cells called crypt base goblet cells (Clevers, 2013; Hou et al., 2020b). Each of these intestinal secretory cell types constitutes an indispensable component of the intestinal mucosal barrier that defends against pathogen infection. The Notch pathway plays a critical role in the differentiation of ISCs toward an intestinal epithelial cell fate by regulating whether a cell differentiates into an absorptive or secretory lineage (Jensen et al., 2000; van Es et al., 2005; Yang et al., 2001). Inhibiting the Notch pathway increases the production of secretory cells at the expense of absorptive enterocytes and colonocytes (Kazanjan et al., 2010; van Es et al., 2010).

The mechanisms by which microbiota interfere with Notch signaling and influence intestinal cell fate are unknown. Studies have linked Notch signaling to Toll-like receptors (TLRs) that detect bacterial components and induce innate immune





(legend on next page)

responses (Palaga et al., 2008; Shang et al., 2016; Zhang et al., 2012) via a conserved adaptor protein, Myd88 (Fre et al., 2011). Others have demonstrated that Myd88-dependent signaling is required for microbiota to promote zebrafish intestinal epithelial proliferation (Cheesman et al., 2011). A notable study demonstrated that modulation of intestinal Notch signaling occurred downstream of microbial signals that promote secretory fates and that the microbiota modulated Notch signaling via Myd88 (Troll et al., 2018). Moreover, our previous study revealed the importance of *L. acidophilus* in preserving homeostatic functions, preventing the progressive loss of goblet cells, and mediating the risk of *Salmonella*-induced colitis through the Notch pathway (Wu et al., 2018).

In this study, we explored the regulatory effects of *Bacillus subtilis* on intestinal epithelial differentiation, particularly secretory cell fate, and its role in protecting the integrity of the intestinal mucosal barrier. We found that live *B. subtilis* stimulated the differentiation of intestinal secretory cells both in intestinal organoids and ileum of mice. These effects were suppressed by the addition of DLL4, indicating that *B. subtilis* inhibited the Notch pathway to reduce the expression of Hes1, thereby shifting ISC differentiation toward a secretory cell fate. Moreover, we demonstrated that the programming effect of *B. subtilis* on intestinal differentiation was TLR2/Myd88 pathway dependent. This study provides evidence that *B. subtilis*-induced, TLR2-dependent signaling plays a role in Notch-mediated intestinal cell fate determination. We also established a model to study the interactions between intestinal microbiota and epithelial cells in a direct manner.

RESULTS

B. subtilis induces the specific expansion of secretory lineage epithelial cells in intestinal organoids

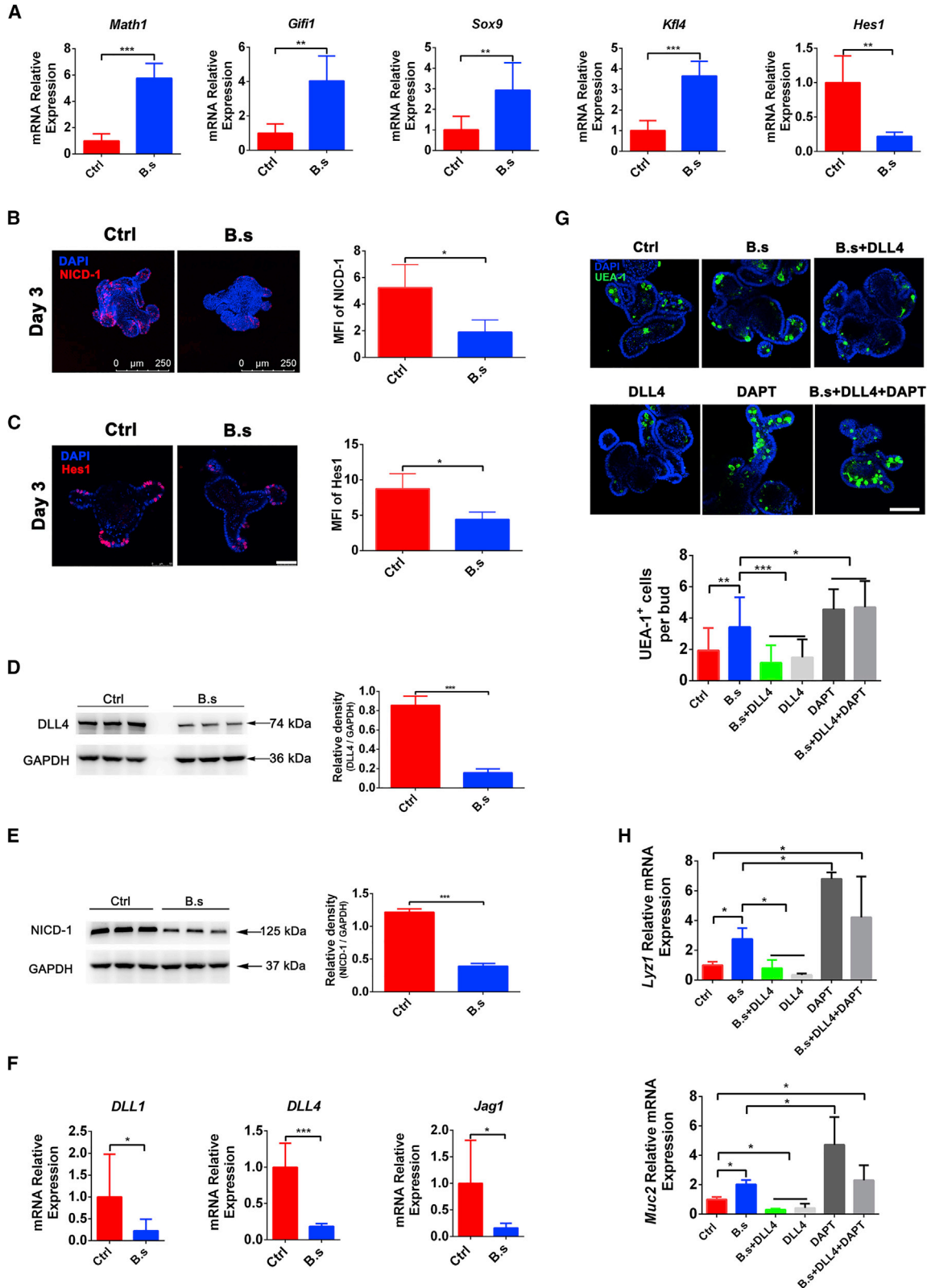
In the small intestine, Paneth cells and mucus-producing goblet cells are most abundant in the ileum. Therefore, small intestinal organoids were isolated from the ileum in all experiments. Based

on an adaptation of previous models (Hou et al., 2018; Lu et al., 2020; Wu et al., 2020), we established a co-culture system consisting of small intestinal organoids and different bacteria to determine their unique roles in the programming of intestinal epithelial differentiation (Figure S1A). Lipoteichoic acid (LTA)/lipopolysaccharide (LPS) antibodies were used to detect the differential capacity of gram-positive and -negative bacteria to attach to small intestinal organoids (Figure S1B). We found that *B. subtilis* 168 and *B. subtilis* WB800 exhibited higher colony counts than the other strains (Figure S1C). After 3 days, we examined the modulatory effect of intestinal microbiota on the fate determination of intestinal epithelial cells in intestinal organoids. Ulex europaeus agglutinin-1 (UEA-1) was used to label intestinal epithelial secretory cells (Mahapatro et al., 2016). Interestingly, treatment with *B. subtilis* 168 and *B. subtilis* WB800 increased the number of UEA-1⁺ cells in the intestinal organoids (Figure 1A). In addition, *B. subtilis* treatment increased the messenger RNA (mRNA) expression of lysozyme 1 (*Lyz1*), mucin 2 (*Muc2*), and chromogranin A (*ChgA*) in small intestinal organoids, which were used as gut-specific markers for Paneth, goblet, and enteroendocrine cells, respectively (Figures 1B–1D). Leucine-rich repeat containing G protein-coupled receptor 5 (Lgr5⁺ ISCs and progenitors were defined as Lgr5-GFP^{hi} cells and Lgr5-GFP^{low} cells in Lgr5-GFP mice, respectively (Sato et al., 2009; Snippert et al., 2010). We first isolated Lgr5⁺ ISCs from Lgr5-GFP mice by fluorescence-activated cell sorting (FACS). Lgr5⁺ ISCs developed into Lgr5-GFP organoids. Flow cytometry analysis showed that *B. subtilis* treatment decreased the number of Lgr5⁺ ISCs and progenitors in Lgr5-GFP organoids more than that seen under other strains treatment (Figure S2A). Additionally, *B. subtilis* treatment decreased expression of Lgr5⁺ ISC marker genes (*Lgr5* and olfactomedin 4 [*Olfm4*]) in Lgr5-GFP organoids (Figure S2B).

We selected *B. subtilis* 168 (hereinafter referred to as *B. subtilis*) as a typical strain to study the role of bacteria on epithelial differentiation fate. Small intestinal organoids were cultured with live or heat-killed (HK) *B. subtilis* for 3 days.

Figure 1. *Bacillus subtilis* induces the specific expansion of secretory lineage cells in mouse small intestinal organoids

- (A) Immunostaining of UEA-1 (green) and DAPI (blue) in the organoids at day 3. Scale bar, 100 μ m. Graph showing UEA-1⁺ cells per organoid bud in different groups; n = 12 organoids per group.
- (B–D) qPCR for markers of intestinal epithelial cell types in small intestinal organoids in different groups: Paneth cell (*Lyz1*), goblet cell (*Muc2*), and enteroendocrine cell (*ChgA*); n = 6.
- (E) Representative pictures of the growth status of organoids stimulated with live or HK *B. subtilis* from 1 to 7 days, as observed by light microscope. Scale bar, 50 μ m. Graph showing the surface area of organoids in different groups; n = 24 organoids per group.
- (F) Immunostaining of UEA-1 (green) and DAPI (blue) in the organoids at day 3. Scale bar, 100 μ m. Graph showing UEA-1⁺ cells per organoid bud in different groups; n = 12 organoids per group.
- (G) Immunostaining of lysozyme (red) and DAPI (blue) in the organoids at day 3. Scale bar, 50 μ m. Graph showing lysozyme⁺ cells per organoid bud in different groups; n = 6 organoids per group.
- (H) Immunostaining of Muc2 (green) and DAPI (blue) in the organoids at day 3. Scale bar, 250 μ m. Graph showing Muc2⁺ cells per organoid bud in different groups; n = 12 organoids per group.
- (I) Immunostaining of Alpi (red) and DAPI (blue) in the organoids at day 3. Scale bar, 250 μ m. Graph showing mean fluorescence intensity (MFI) of Alpi in different groups; n = 6 organoids per group.
- (J) Immunostaining of Lgr5 (green) and DAPI (blue) in the organoids at day 3. Scale bar, 75 μ m. Graph showing MFI of Lgr5 in different groups; n = 6 organoids per group.
- (K) Immunostaining of EdU (red) and DAPI (blue) in the organoids at day 3. Scale bar, 50 μ m. Graph showing MFI of EdU in different groups; n = 6 organoids per group.
- (L) qPCR for markers of intestinal epithelial cell types in organoids in different groups: *Lyz1*, *Muc2*, *ChgA*, absorptive enterocyte (*Alpi*), and Lgr5⁺ ISC (*Lgr5*). Data are the mean \pm SD; comparisons performed with t tests (two groups) or analysis of variance (ANOVA) (multiple groups). *p < 0.05, **p < 0.01, ***p < 0.001. Results are representative of three independent experiments.



(legend on next page)

Immunofluorescence (IF) staining and plate counting showed that only live *B. subtilis* attached to the organoids (Figure S1D) and grew in the co-culture system (Figure S1E). HK *B. subtilis* lost its ability to attach to the organoid (Figure S1D). No changes in the surface area of the intestinal organoids were observed from day 1 to day 7 (Figure 1E). After 3 days, we examined the number of secretory cells in the intestinal organoids. Interestingly, treatment with live *B. subtilis* significantly increased the number of UEA-1⁺ cells in small intestinal (Figure 1F) and colonic organoids (Figure S3A). Moreover, IF staining demonstrated that live *B. subtilis* treatment increased the number of lysozyme⁺ Paneth cells (Figure 1G) and Muc2⁺ goblet cells (Figure 1H). Treatment with *B. subtilis* also significantly increased the mRNA expression of *Lyz1*, *Muc2*, and *ChgA* in small intestinal organoids (Figure 1L) and of *Muc2* in colonic organoids (Figure S3B). In contrast, IF staining and qPCR analysis showed that *B. subtilis* treatment decreased expression of the enterocyte marker alkaline phosphatase (*Alpi*) and *Lgr5* (Figures 1I, 1J, and 1L). 5-Ethynyl-2'-deoxyuridine (EdU) was used to label proliferating cells (Buck et al., 2008). Interestingly, we observed a lower percentage of EdU⁺ cells in the organoids treated with live *B. subtilis* (Figure 1K). However, HK *B. subtilis* did not exhibit a stimulatory effect on the programming of intestinal epithelial differentiation. These results indicated that live *B. subtilis* inhibited the proliferation of Lgr5⁺ ISCs but significantly promoted the differentiation toward the secretory cell line.

***B. subtilis* regulates intestinal cell fate determination by inhibiting the Notch pathway**

Early expression of key transcription factors, such as Hes1 and Math1, is known to direct intestinal epithelial differentiation toward two major lineages, either absorptive or secretory (Gazit et al., 2004; Mahapatro et al., 2016). Because our model showed a specific increase in secretory lineage cells, we hypothesized that *B. subtilis* might regulate the expression of these differentiation factors. Indeed, we observed that the mRNA expression of the early differentiation markers *Math1*, growth factor independent 1 transcriptional repressor (*Gfi1*), SRY-box transcription factor 9 (*Sox9*), and Kruppel-like factor 4 (*Klf4*) were higher, whereas the expression levels of *Hes1* were lower, in organoids treated with *B. subtilis* than in controls (Figure 2A). Because the Notch pathway has been demonstrated to promote the expres-

sion of Hes family genes and to repress the expression of Math1 (Tsai et al., 2014), we hypothesized that *B. subtilis* programs epithelial differentiation by regulating Notch signaling. Immunostaining revealed that NICD-1 and Hes1 proteins were abundantly expressed in small intestinal organoids in the control group, but their expression was downregulated in the *B. subtilis* group (Figures 2B and 2C). These findings were further supported by western blot analyses showing that the intensities of both DLL4 and NICD1 bands were lower in small intestinal organoids treated with *B. subtilis* than in controls (Figures 2D and 2E). Moreover, qPCR analysis showed that the expression of the Notch ligands *Dll1*, *Dll4*, and *Jag1* was lower in small intestinal organoids treated with *B. subtilis* than in the control (Figure 2F).

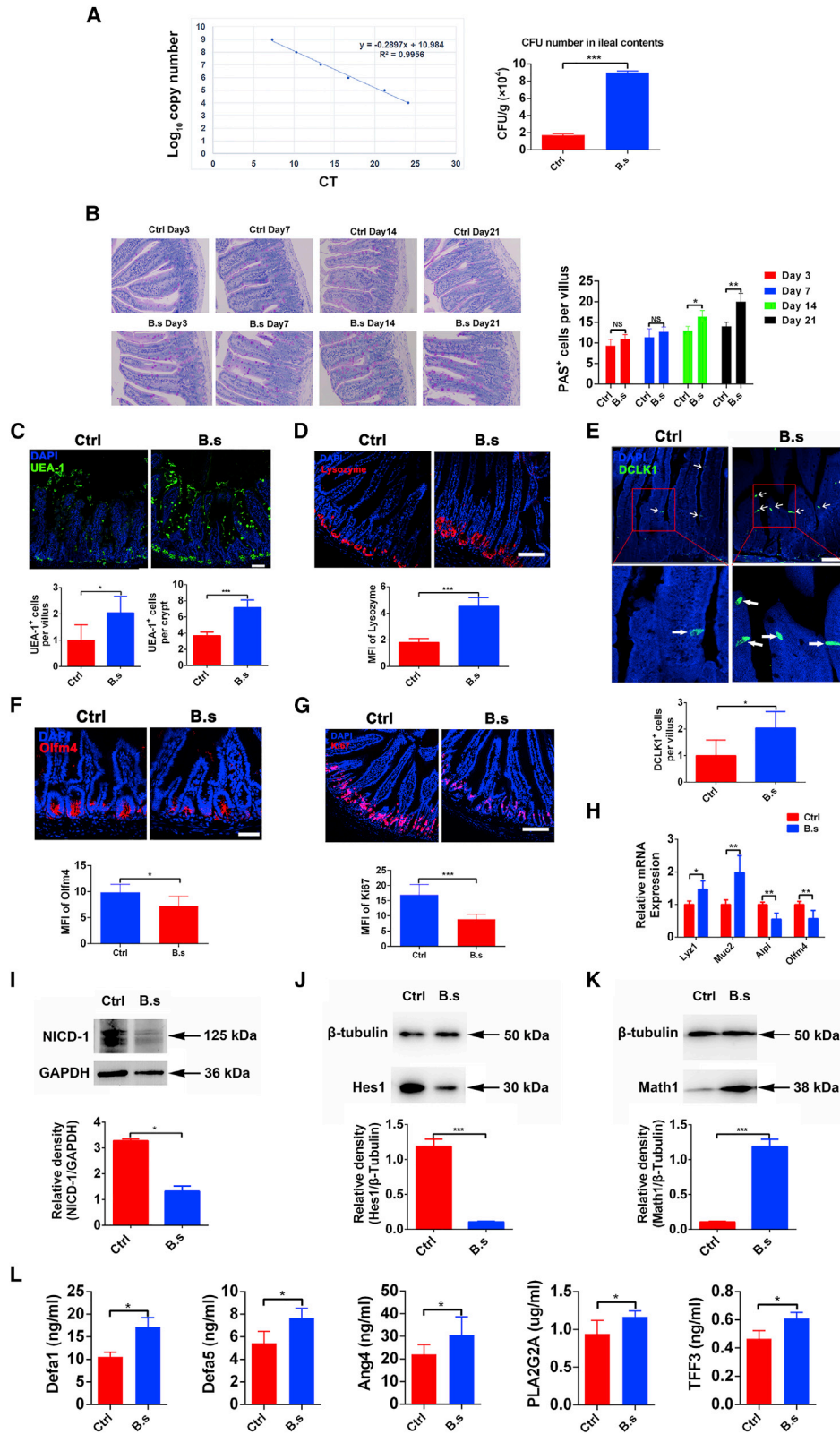
Paneth cells express the Notch ligands *Dll1*, *Dll4*, and *Jag1*. We isolated CD24⁺SSC^{hi} Paneth cells from the small intestinal organoids or ilea of mice treated with *B. subtilis* (Figure S7A). qPCR analyses showed that *B. subtilis* treatment decreased the expression levels of *Dll1*, *Dll4*, and *Jag1* in these Paneth cells (Figure S7B) and in the ileal crypts (Figure S7C). To investigate whether Notch signaling is functionally involved in epithelial responses to *B. subtilis*, we treated *B. subtilis*-stimulated intestinal organoids with or without the Notch ligand DLL4 or the Notch inhibitor N-[N-(3, 5-difluorophenacetyl)-L-alanyl]-S-phenylglycine-butylester (DAPT). Intestinal organoids that were treated with either *B. subtilis* or DAPT developed more UEA-1⁺ secretory cells (Figure 2G). However, the addition of DLL4 completely blocked *B. subtilis*-induced expansion of secretory cells (Figure 2G) and decreased the mRNA expression of *Lyz1* and *Muc2* (Figure 2H). Collectively, these data demonstrate that *B. subtilis* inhibited Notch signaling to promote the reprogramming of intestinal epithelial differentiation toward a secretory cell fate *in vitro*.

***B. subtilis* modulates the differentiation of secretory lineage cells in mice**

Mice were administered phosphate-buffered saline (PBS; 200 μ L) or 10⁸ colony-forming units (CFUs) of *B. subtilis* suspended in 200 μ L of PBS once per day for a period of 21 days. *B. subtilis* colonization in the intestine of mice treated with or without *B. subtilis* on day 21 was then analyzed by qPCR and plate counting. Higher *B. subtilis* abundance was found in the ileal contents of mice treated with *B. subtilis* than in those of the control group, according to the standard curve of bacteria

Figure 2. *B. subtilis* regulates intestinal cell fate decisions by inhibiting Notch signaling

(A–F) Small intestinal organoids were treated with live *B. subtilis* 168 for 3 days.
(A) qPCR analysis of early the differentiation marker genes *Hes1*, *Math1*, *Gfi1*, *Sox9*, and *Klf4* in the organoids; n = 6.
(B and C) Immunostaining of NICD-1 (red) and DAPI (blue) in the organoids at day 3. Scale bar, 250 μ m. Graph showing MFI of NICD-1 in different groups; n = 12 organoids per group.
(C) Immunostaining of Hes1 (red) and DAPI (blue) in the organoids at day 3. Scale bar, 50 μ m. Graph showing MFI of Hes1 in different groups; n = 12 organoids per group.
(D and E) Western blot analysis of DLL4 and NICD-1 expression in the organoid lysates; GAPDH was used as a loading control. Graph showing the quantification of DLL4 and NICD-1 levels in different groups; n = 3.
(F) qPCR analysis of the Notch ligands *Dll1*, *Dll4*, and *Jag1* in intestinal organoids; n = 6.
(G and H) Small intestinal organoids were treated with *B. subtilis*, DLL4, a Notch inhibitor (DAPT), and their combinations for 3 days.
(G) Immunostaining of UEA-1 (green) in the organoids at day 3. Scale bar, 50 μ m. Graph quantifying UEA-1⁺ cells per organoid bud in different groups; n = 24 organoids per group.
(H) qPCR analysis of *Lyz1* and *Muc2* in the organoids.
Data represent the mean \pm SD of three independent experiments; comparisons performed with t tests (two groups) or ANOVA (multiple groups). *p < 0.05, **p < 0.01, ***p < 0.001.



(legend on next page)

(Figure 3A) and plate counting (Figure S4A). Moreover, these results indicated that *B. subtilis* was effectively delivered to the small intestine of the treated mice. *B. subtilis* treatment was associated with increased villus height and crypt depth but decreased the villus:crypt ratio in the ileum (Figure S5A). Subsequently, we examined the effect of *B. subtilis* on secretory cell differentiation in the ileum from day 1 to day 21 *in vivo*. Treatment with *B. subtilis* was associated with a significant increase in the number of periodic acid-Schiff (PAS)⁺ cells in the ileum at day 21 (Figure 3B). Moreover, IF staining demonstrated that *B. subtilis* significantly increased the number of UEA-1⁺ intestinal secretory cells (Figure 3C) and lysozyme⁺ Paneth cells (Figure 3D). Tuft cells, which are taste-chemosensory epithelial cells, accumulate during parasite colonization and infection. IF staining showed an increase in tuft cells in the ileum of mice treated with *B. subtilis* (Figure 3E). Olfm4 can serve as a useful marker for Lgr5-type stem cells in the small intestine (van der Flier et al., 2009). IF staining in *B. subtilis*-treated mice showed decreased expression of *Olfm4* (Figure 3F) and the cell proliferation marker *Ki67* (Figure 3G) in the ileum. Moreover, qPCR analyses showed that *B. subtilis* treatment increased the expression levels of *Lyz1* and *Muc2* but decreased the levels of *Alpi* and *Olfm4* in ileum (Figure 3H). Western blot analyses showed that the intensity of NICD-1 and Hes1 bands was lower in the ilea of mice treated with *B. subtilis* than in those of the control group (Figures 3I and 3J). However, ileal *Math1* protein expression was higher in the *B. subtilis* group than in the control group (Figure 3K). Paneth cells limit bacterial invasion by secreting antimicrobial peptides (AMPs; including lysozyme; α -defensins, such as defensin a1 [Defa1] and Defa5; angiogenin 4 [Ang4]; and PLA2G2A; Bevins and Salzman, 2011). Trefoil factor family 3 (TFF3) is the second most abundant goblet cell product behind mucins and facilitates not only intestinal epithelial restitution but also mucosal protection (Kim and Ho, 2010). We found that lysozyme, Ang4, and TFF3 limited the invasion of *Salmonella typhimurium* into Caco-2 cells in a dose-dependent manner (Figures S6A and S6B). Notably, treatment with *B. subtilis* increased the expression of these AMPs (Defa1, Defa5, Ang4, PLA2G2A, and TFF3) in the ileum (Figure 3L). Overall, these results show that *B. subtilis* modulated the differentiation of secretory lineage cells through the Notch signaling pathway *in vivo*.

TLR2-Myd88-dependent signaling is essential for the *B. subtilis*-induced expansion of secretory cells

To determine the role of TLR2 in *B. subtilis*-mediated inhibition of Notch signaling, we first obtained small intestinal organoids from wild-type (WT) and TLR2^{-/-} mice. IF staining and western blot

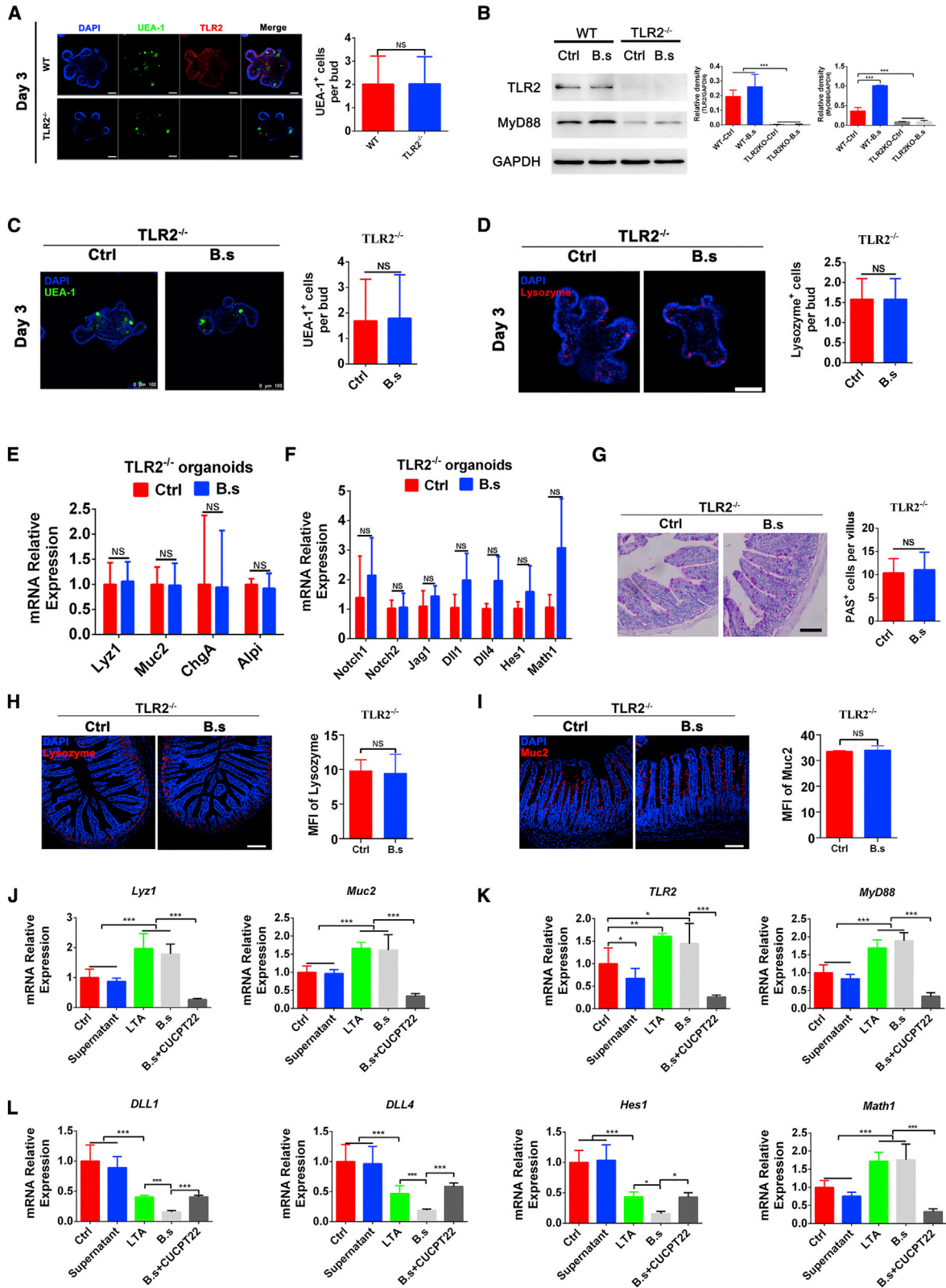
analyses showed that the TLR2 protein was abundantly expressed in the organoids from WT mice but was not detected in the TLR2^{-/-} organoids (Figures 4A and 4B). In addition, TLR2 knockout did not alter the number of UEA-1⁺ intestinal secretory cells, neither *in vitro* (Figure 4A) nor *in vivo* (Figure S5B). Western blot analyses showed that the intensity of the bands for MyD88 increased in the organoids obtained from WT mice treated with *B. subtilis* but not in those from the TLR2^{-/-} group (Figure 4B). Furthermore, we found that *B. subtilis* induced the specific expansion of secretory lineage cells. Strikingly, no increase was seen in the number of UEA-1⁺ and lysozyme⁺ cells nor in the mRNA expression of secretory cell markers in TLR2^{-/-} organoids stimulated with *B. subtilis* (Figures 4C–4E). Although the differences were not significant ($p > 0.05$), the expression of Notch-related genes (*Notch1*, *Notch2*, *Jag1*, *Dll1*, *Dll4*, *Hes1*, and *Math1*) showed a rising trend in the TLR2^{-/-} organoids stimulated with *B. subtilis* (Figure 4F). Treatment with *B. subtilis* did not alter the number of PAS⁺, lysozyme⁺, or Muc2⁺ cells in the ileum of TLR2^{-/-} mice (Figures 4G–4I). To further explore the role of TLR2-Myd88-dependent signaling, we treated small intestinal organoids from WT mice with *B. subtilis*, *B. subtilis* culture supernatant, a TLR2 agonist (LTA), a TLR2 inhibitor (CUCPT22), and their combinations for 3 days. Interestingly, both *B. subtilis* and LTA treatment increased the mRNA expression of *Lyz1*, *Muc2*, *TLR2*, *MyD88*, and *Math1* (Figures 4J–4L) but significantly downregulated the expression of Notch-related genes (*Dll1*, *Dll4*, and *Hes1*) (Figure 4L). However, CUCPT22 treatment resulted in the opposite expression patterns (Figures 4J–4L). Collectively, these data demonstrate that TLR2-Myd88-dependent signaling is essential for *B. subtilis*-induced expansion of secretory cells.

S. typhimurium infection and invasion in intestinal organoids

To build an intestinal organoid culture system to represent salmonellosis, we first infected intestinal organoids with pathogenic *S. typhimurium* SL1344. As shown in Figure 5A, we found that *S. typhimurium* infection led to the disruption of normal organoid morphology, with a large number of dead cells seen under a light microscope. We further found that a large number of *S. typhimurium* cells had invaded the organoids (Figure 5B). To visualize the invasion of *S. typhimurium* into small intestinal organoids, we colonized the cultures with fluorescence-labeled *S. typhimurium* for 90 min. Green fluorescence-labeled *S. typhimurium* attached to and invaded the organoids (Figure 5C). Moreover, ELISA data showed that the levels of the inflammatory cytokines interleukin-1 β (IL-1 β) and tumor necrosis

Figure 3. *B. subtilis* induces the specific expansion of secretory lineage cells *in vivo*

(A–I) Mice were orally administered *B. subtilis* 168 (1×10^8 CFUs) or PBS once a day for 21 days. (A) *B. subtilis* 168 in the ileal contents (right panel). The CFU number was determined by qPCR according to the standard curve of *B. subtilis* (left panel). (B) Representative pictures of PAS staining in the ileum from day 1 to day 21. Scale bar, 50 μ m. Graph showing PAS⁺ cells per villus; n = 6 mice per group. (C–G) Immunostaining of UEA-1 (green), lysozyme (red), DCLK1 (green), Olfm4 (red), Ki67 (red), and DAPI (blue) in the ileum at day 21. Scale bar, 50 μ m. Graph showing UEA-1⁺ cells per villus or crypt and MFI of lysozyme (red), Olfm4 (red), and Ki67 (red); n = 6 mice per group. (H) qPCR analysis of ileal *Lyz1*, *Muc2*, *Alpi*, and *Olfm4*. (I–K) Western blot analysis of ileal NICD-1, Hes1, and Math1 expression. GAPDH and β -tubulin were used as loading controls; n = 3 mice per group. (L) ELISA of antimicrobial peptides (Defa1, Defa5, Ang4, and PLA2G2A) and TFF3 expression in the ileum. Data represent the mean \pm SD of three independent experiments; comparisons performed with t tests (two groups). * $p < 0.05$, ** $p < 0.01$, *** $p < 0.001$.



(legend on next page)

factor α (TNF- α) were higher in the culture medium at 12 h post-infection (Figures 5D and 5E).

***B. subtilis* protects the intestinal barrier against *S. typhimurium* infection by increasing secretory cell levels**

Paneth and goblet cells are important secretory epithelial cells with innate immune functions and roles in defense against enteric pathogens (Lievin-Le Moal and Servin, 2006). Indeed, *B. subtilis*-treated intestinal organoids exhibited increased levels of lysozyme and Muc2, which are markers of Paneth and goblet cells, respectively. These findings were further supported by qPCR analyses of AMPs produced by Paneth and goblet cells in small intestinal organoids, including *Defa1*, *Defa5*, *Ang4*, *PLA2G2A*, and *TFF3* (Figure 6A). Small intestinal organoids were treated with *B. subtilis*, DLL4, and *S. typhimurium* according to the methods described in Figure 6B. Briefly, the organoids were first treated with or without *B. subtilis* and DLL4 for 3 days. Interestingly, the *Salmonella* burden was lower at 12 h post-infection in the organoids treated with *B. subtilis* alone than in the control and DLL4 plus *B. subtilis* groups (Figures 6E and 6F). Moreover, the number of disrupted organoids was significantly lower in the *B. subtilis* group, and this was reversed by addition of DLL4 (Figures 6C and 6D). Moreover, ELISA data showed that at 12 h post-infection, the levels of IL-1 β and TNF- α were significantly lower in the culture medium of the *B. subtilis* group than in those of the control and DLL4 plus *B. subtilis* groups (Figure 6G). Moreover, *B. subtilis* treatment decreased the number of disrupted organoids (Figure S3C) and *S. typhimurium* invasion in colonic organoids (Figure S3D). Collectively, these data suggest that *B. subtilis* protected the gut from *S. typhimurium* infection and promoted epithelially mediated antimicrobial defenses.

***B. subtilis* provides protection against the pathogen *S. typhimurium* in mice**

To further clarify the protective role of *B. subtilis*, mice were orally administered *B. subtilis* (1×10^8 CFUs) or PBS once a day for

21 days. Mice were orally administered *S. typhimurium* strain 1344 (1×10^8 CFUs) once, on day 14. *S. typhimurium* infection caused a reduction in body weight in the control group, but this affect was attenuated in the group administered *B. subtilis* (Figure 7A). The protective effect of *B. subtilis* against *S. typhimurium* was also demonstrated by survival testing of mice (Figure 7B) and intestine length (Figure 7C). Hematoxylin and eosin (H&E) staining showed that *Salmonella* infection decreased ileal villus height and crypt depth in the control group but not in the *B. subtilis* group (Figure 7D). Moreover, *B. subtilis* treatment increased AMP expression (*Defa1*, *Defa5*, *Ang4*, *PLA2G2A*, and *TFF3*) in the ileum of mice infected with *S. typhimurium* (Figure 7E). *B. subtilis* treatment also reduced LPS concentration in the serum (Figure 7F) and secreted levels of proinflammatory cytokines (IL-1 β and TNF- α) in the ileum (Figures 7G and 7H). We also found that treatment with *B. subtilis* reduced the burden of *S. typhimurium* in feces (Figure 7I). Collectively, these results indicated that intragastric administration of *B. subtilis* improved mouse resistance against *S. typhimurium* infection. These findings led us to ask whether the protective effect of *B. subtilis* is mediated by an increase in secretory cells. *S. typhimurium* infection induced a significant loss in the number of secretory goblet and Paneth cells in the ileum (Figures 7J and 7K). However, treatment with *B. subtilis* significantly alleviated this loss (Figures 7J and 7K). Moreover, qPCR analyses showed that the expression levels of Notch signaling-related genes (*Notch1*, *Dll1*, *Dll4*, *Jag1*, and *Hes1*) were lower in the ileum of mice treated with *B. subtilis* (Figure 7L). Overall, these results demonstrated that *B. subtilis* provided protection against the pathogen *S. typhimurium* in mice through a mechanism mediated, at least in part, by Notch signaling.

DISCUSSION

Host-associated microbiota play critical roles in animal health and development (Kundu et al., 2017); the mechanisms by which they influence processes, such as cell differentiation, remain

Figure 4. TLR2 is essential for *B. subtilis*-induced secretory cell expansion

(A–F) Small intestinal organoids from TLR2^{-/-} mice were treated with live *B. subtilis* 168 for 3 days.

(A) Immunostaining of TLR2 (red), UEA-1 (green), and DAPI (blue) in the organoids at day 3. Scale bar, 50 μ m. Graph quantifying UEA-1⁺ cells per organoid bud; n = 12 organoids per group.

(B) Western blot analysis of TLR2 and MyD88 expression in the organoid lysates; GAPDH was used as a loading control. Graph quantifying TLR2 and MyD88; n = 3.

(C) Immunostaining of UEA-1 (green) and DAPI (blue) in the organoids at day 3. Scale bar, 100 μ m. Graph showing UEA-1⁺ cells per organoid bud; n = 12 organoids per group.

(D) Immunostaining of lysozyme (red) and DAPI (blue) in the organoids at day 3. Scale bar, 50 μ m. Graph showing lysozyme⁺ cells per organoid bud; n = 12 organoids per group.

(E) qPCR analysis of intestinal epithelial cell marker genes (*Lyz1*, *Muc2*, *ChgA*, and *Alpi*); n = 6.

(F) qPCR analysis of Notch-related genes (*Notch1*, *Notch2*, *Jag1*, *Dll1*, *Dll4*, *Hes1*, and *Math1*) in the organoids; n = 6.

(G–I) TLR2^{-/-} mice were orally administered *B. subtilis* 168 (1×10^8 CFUs) or PBS as a control once a day for 21 days.

(G) Representative pictures of ileal PAS staining at day 21. Scale bar, 50 μ m. Graph showing PAS⁺ cells per villus; n = 6 mice per group.

(H and I) Immunostaining of lysozyme (red), Ki67 (red), and DAPI (blue) in the ileum at day 3. Scale bar, 50 μ m. Graph showing MFI of lysozyme and Muc2; n = 6 mice per group.

(H–J) Small intestinal organoids from WT mice were treated with *B. subtilis*, *B. subtilis* culture supernatant, a TLR2 agonist (lipoteichoic acid, LTA), a TLR2 inhibitor (CUCPT22), and their combinations for 3 days.

(J and K) qPCR analysis of *Lyz1*, *Muc2*, *TLR2*, and *MyD88* in the organoids; n = 6.

(L) qPCR analysis of Notch-related genes (*Dll1*, *Dll4*, *Hes1*, and *Math1*) in the organoids; n = 6.

Data represent the mean \pm SD of three independent experiments; comparisons performed with t tests (two groups) or ANOVA (multiple groups). *p < 0.05, **p < 0.01, ***p < 0.001.

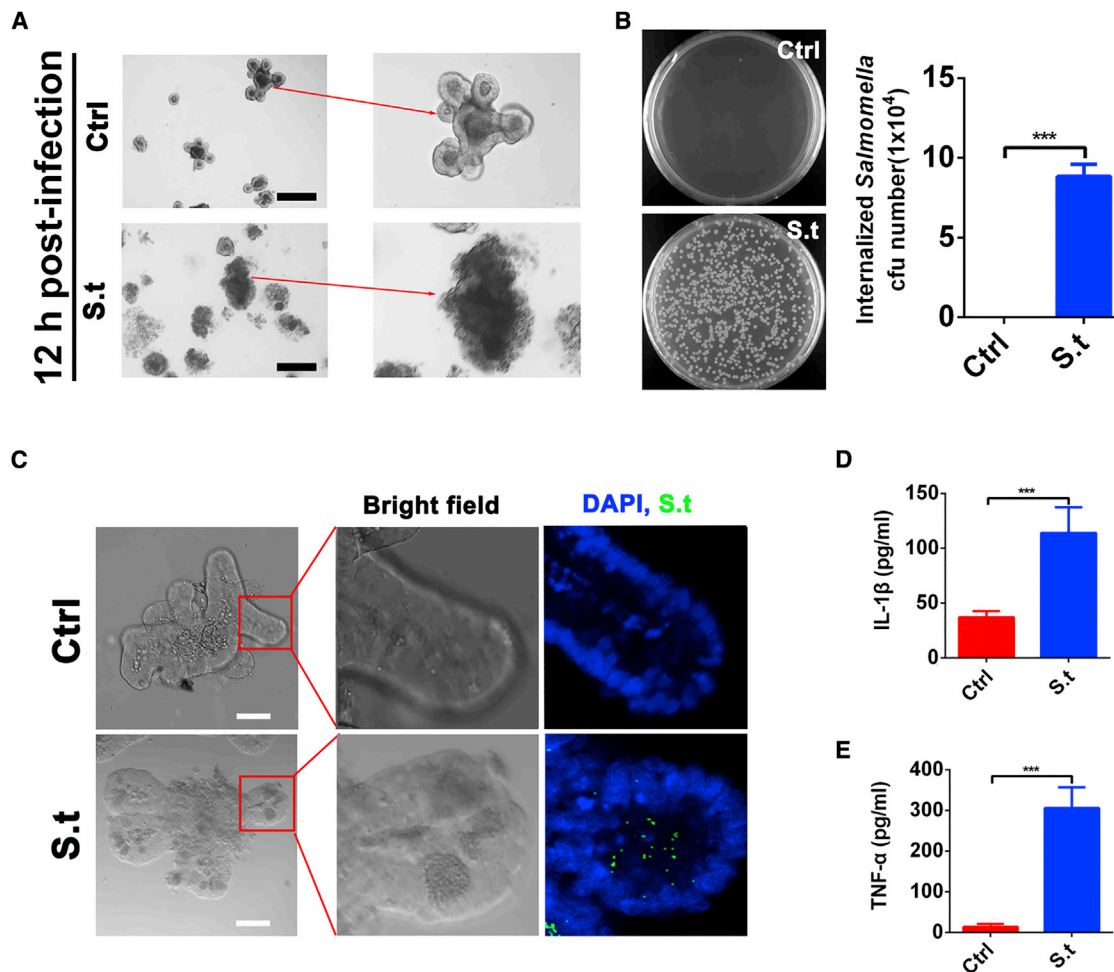


Figure 5. *Salmonella typhimurium* infection and invasion in mouse small intestinal organoids

(A) Micrographs showing representative small intestinal organoids, infected or not infected with *S. typhimurium*. Scale bar, 200 μ m. (B) Quantification of invasive *Salmonella* cells per well in the organoids colonized with or without *Salmonella* at 12 h post-infection; n = 6. (C) *Salmonella* (green) attached to and invaded the organoids. Scale bar, 50 μ m. (D and E) ELISA of inflammatory cytokine (TNF- α and IL-1 β) levels in culture medium at 12 h post-infection; n = 6. Data represent the mean \pm SD of three independent experiments; comparisons performed with t tests (two groups). *p < 0.05, **p < 0.01, ***p < 0.001.

unknown. A system called mini-gut organoid culture has been introduced in previous studies (Mahe et al., 2013; Sato et al., 2009). Studies using intestinal organoids have advanced our understanding of host-microbiota interactions and development of the intestines. Co-culture strategy of organoids and microbe have been summarized and described in a recent review (Puschhof et al., 2021). Microbes can be microinjected into organoids, added during organoid shearing, or added to monolayers grown from cell lines, organoids, or explants (Puschhof et al., 2021). The method we used is to add bacteria during organoid shearing. In our present study, we established a co-culture system of intestinal organoids and different bacteria to determine the role of different bacteria in the programming of intestinal epithelial differentiation. To ensure that all co-cultures were successful, we addressed the differential capacity of the strains to attach to the organoids. IF staining showed that *B. subtilis* 168, *B. subtilis* WB800, *Lactobacillus acidophilus* ATCC4356, and

E. coli successfully attached to the organoids. All the strains grew well in the organoids. Moreover, we found that *B. subtilis* 168 and *B. subtilis* WB800 grew more successfully than the other strains in the organoids. This may be due to the characteristics and oxygen demand of the different bacteria.

ISCs continuously self-renew and give rise to progenitors (transit-amplifying cells), which undergo additional cell divisions prior to terminal differentiation and maturation (van der Flier and Clevers, 2009). By building organoid-*Lactobacillus* co-culture models, we previously showed that the *Lactobacillus* could accelerate ISC-mediated intestinal epithelial development (Hou et al., 2018; Lu et al., 2020; Wu et al., 2020). Interestingly, treatment with *B. subtilis* increased the number of secretory Paneth and goblet cells. Nevertheless, *B. subtilis* treatment decreased the number of Lgr5⁺ ISCs, progenitor cells, and absorptive lineage cells. Moreover, we observed a lower percentage of EdU⁺ cells in organoids treated with *B. subtilis*. Collectively, these

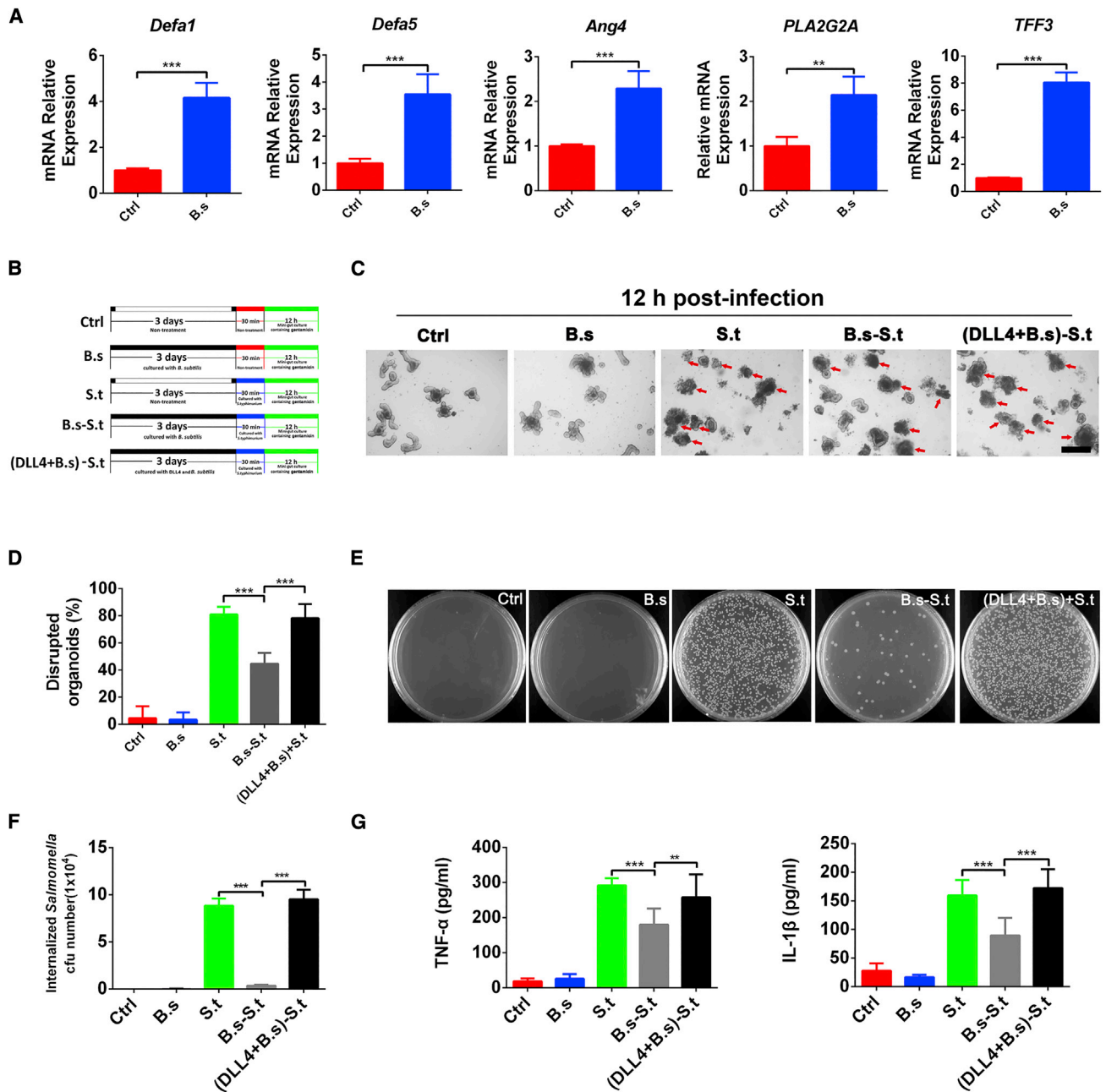


Figure 6. *B. subtilis* provides protection against the pathogen *S. typhimurium* in mouse small intestinal organoids

(A) qPCR analysis of the levels of antimicrobial peptides (*Defa1*, *Defa5*, *Ang4*, and *PLA2G2A*) and *TFF3* in small intestinal organoids with or without *B. subtilis* stimulation; n = 6.

(B) Different treatment methods used in each group (Ctrl, B.s, S.t, B.s-S.t, and (DLL4+B.s)-S.t).

(C) The morphology of the organoids in different groups was observed with a light microscope at 12 h post-infection. Scale bar, 200 μ m.

(D) The relative number of disrupted organoids (red arrow) in the different groups at 12 h post-infection; n = 6.

(E) Photo used to determine plate counts in the different groups (Ctrl, B.s, S.t, B.s-S.t, and (DLL4+B.s)-S.t) at 12 h post-infection.

(F) Number of invasive *Salmonella* in the organoids at 12 h post-infection; n = 6.

(G) ELISA of inflammatory cytokine (TNF- α and IL-1 β) levels in culture medium at 12 h post-infection; n = 6.

Data represent the mean \pm SD of three independent experiments; comparisons performed with t tests (two groups) or ANOVA (multiple groups). *p < 0.05, **p < 0.01, ***p < 0.001.

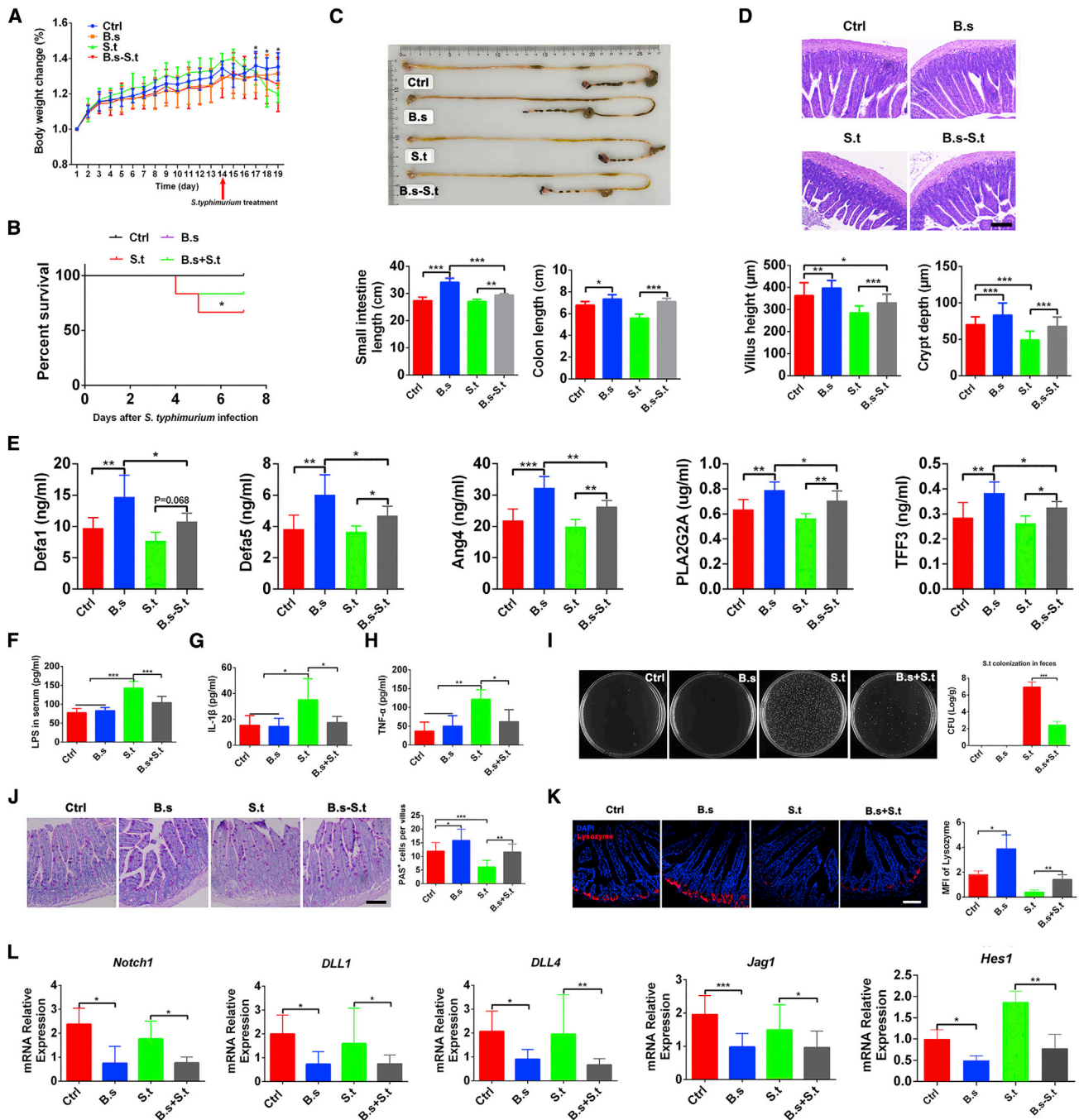


Figure 7. *B. subtilis* provides protection against the pathogen *S. typhimurium* in mice

Mice were orally administered *B. subtilis* 168 (1×10^8 CFUs) or PBS as a control once a day for 21 days. Some mice were orally administered *S. typhimurium* strain 1344 (1×10^8 CFUs) once on day 14.

(A) Changes in body weight were monitored daily starting from day 1 to day 19 and presented relative to the initial body weight; $n = 6$.

(B) Time course of mouse survival; $n = 6$.

(C) Representative pictures of mouse intestines. Graph showing small intestine and colon lengths; $n = 6$ mice.

(D) Representative pictures of H&E staining in the ileum. Scale bar, 100 μm. Graph showing villus height and crypt depth; $n = 6$.

(E) ELISA of antimicrobial peptides (Defa1, Defa5, Ang4, and PLA2G2A) and TFF3 expression in the ileum; $n = 6$.

(F–H) ELISA of LPS in the serum and IL-1β and TNF-α in the ileum; $n = 6$.

(I) *Salmonella* burden in the feces, as determined by streptomycin agar plates at 7 days post-infection. Figure shows the CFU per gram of fecal sample; $n = 6$.

(J) Representative images of PAS staining in the ileum at day 21. Scale bar, 50 μm. Graph showing PAS⁺ cells per villus; $n = 6$.

(legend continued on next page)

data support the hypothesis that *B. subtilis* induces a programming effect whereby ISCs differentiate toward a secretory cell fate at the expense of absorptive enterocytes and proliferation. However, due to the lack of lineage tracing experiments, other mechanisms independent of ISC function may be involved in the differentiation of intestinal secretory lineages by *B. subtilis*.

The activities of ISCs are tightly regulated by several niche-signaling pathways, including Wnt/ β -catenin, the Notch pathway, and BMP signaling, such that intestinal homeostasis is appropriately balanced under various physiological and pathological conditions (Gehart and Clevers, 2019). Notch signaling is a key mechanism for cell fate determination throughout the animal kingdom (Siebel and Lendahl, 2017). Unlike other stem cells, ISCs co-exist with intestinal microbiota, which may influence differentiation of the epithelium (Siebel and Lendahl, 2017). Therefore, we utilized both organoid and mouse models to test whether *B. subtilis* influences secretory fate via Notch signaling. We demonstrated that *B. subtilis* inhibits Notch pathway signaling by reducing the expression of Notch ligands and target genes (Hes1), both *in vivo* and *in vitro*. Paneth cells express Notch ligands, such as Dll1, Dll4, and Jag1. In our experiment, we found that the expression of Notch ligand genes decreased upon *B. subtilis* treatment, although the number of Paneth cells increased. However, the number of ligands expressed by Paneth cells decreased. To verify our findings, we isolated CD24⁺SSC^{hi} Paneth cells from the small intestinal organoids or ilea of mice treated with *B. subtilis*. qPCR analyses showed that *B. subtilis* treatment decreased the expression levels of *Dll1*, *Dll4*, and *Jag1* in these Paneth cells. Moreover, *B. subtilis* increased the expression of lineage-specific transcription factors, such as *Math1*, *Sox9*, and *Gfi1*, which are required for the proper differentiation of secretory cells (van der Flier and Clevers, 2009). These results suggest that *B. subtilis* inhibits the Notch pathway and induces an increase in secretory cell counts.

The mechanisms by which microbiota interact with the Notch signaling pathway and influence intestinal cell fate are largely unknown. TLRs play a crucial role in recognizing microbial components via the innate immune system. The microbe-associated molecular patterns (MAMPs) on the surfaces of *B. subtilis* cells contain peptidoglycans, such as LTA and wall teichoic acid, which are predominantly detected by TLR2 (Lebeer et al., 2010). Studies have linked Notch signaling to TLRs, which detect bacterial components and induce innate immune responses (Palaga et al., 2008; Shang et al., 2016; Zhang et al., 2012) via a conserved adaptor protein, Myd88 (Fre et al., 2011). Additionally, Troll et al. demonstrated that modulation of intestinal Notch signaling occurs downstream of microbial signals that promote secretory fates and that microbiota modulate Notch signaling via Myd88 (Troll et al., 2018). These studies have indicated that TLR2 signals may be involved in the differentiation of intestinal secretory lineages by *B. subtilis* through the Notch pathway. Utilizing TLR2^{-/-} mice and a TLR2 inhibitor,

our results showed that the MAMP-LTAs from *B. subtilis* participated, at least in part, in the process of inhibition of Notch signaling in a TLR2-MyD88-dependent manner. Our research answers the question, to some extent, of how *B. subtilis* affects Notch signaling. We look forward to revealing the specific mechanisms in future research.

The mucus layer and the AMPs overlying the epithelium are secreted by goblet cells and Paneth cells and promote the elimination of gut contents, representing the first line of defense against physical and chemical injury caused by ingested food, microbes, and microbial products (Bevins and Salzman, 2011; Birchenough et al., 2015). Paneth cells produce a variety of AMPs, such as lysozyme, α -defensins, Ang4, and PLA2G2A. MUC2 is the major secretory mucin synthesized and secreted by goblet cells into the intestines. TFF3 blocks apoptosis and contributes to the innate immune response mediated by the mucosal sensor systems of the commensal microbiota. These two goblet cell products not only facilitate intestinal epithelial restitution but also promote mucosal protection (Kim and Khan, 2013; Kim and Ho, 2010). Moreover, we selected several products of Paneth cells and goblet cells such as lysozyme, Ang4, and TFF3 and verified the resistance of these products to *S. typhimurium*. We found that lysozyme, Ang4, and TFF3 limited the invasion of *S. typhimurium* into intestinal epithelial cells in a dose-dependent manner. *S. typhimurium* infection damaged epithelial cells and increased the secretion of TNF- α and IL-1 β both *in vivo* and *in vitro*. However, *B. subtilis* treatment significantly increased the number of Paneth cells, goblet cells, and AMPs, defending against *S. typhimurium* infection. Treatment with DLL4 eliminated this protective effect against *S. typhimurium* infection, indicating that the ability of *B. subtilis* to inhibit Notch pathway signaling is essential to maintain the integrity of the intestinal mucosal barrier.

In conclusion, we demonstrated that *B. subtilis* inhibits Notch pathway signaling, programs intestinal epithelial cells to differentiate toward a secretory cell fate, and increases the production of mucins and AMPs to defend against *S. typhimurium* infection. Moreover, we showed that the regulatory effect of *B. subtilis* on epithelial differentiation is TLR2 dependent. Therefore, the results of this study indicate that probiotic components of the intestinal microbiota, such as *B. subtilis*, affect ISC differentiation and proliferation to protect the mucosal barrier. However, how *B. subtilis* acts on TLR2 and affects the Notch signaling pathway remains unclear. Our previous study clarified that the *Lactobacillus reuteri* metabolite indole-3-aldehyde stimulated lamina propria lymphocytes to secrete IL-22 through the aryl hydrocarbon receptor, inducing phosphorylation of STAT3 to accelerate proliferation of ISCs (Hou et al., 2018). Moreover, another study demonstrated that microbiota-derived lactate accelerated ISC-mediated epithelial development in mice (Lee et al., 2018). The finding that *B. subtilis* can modulate host intestinal epithelial Notch

(K) Immunostaining of lysozyme (red) and DAPI (blue) in the ileum at day 21. Scale bar, 50 μ m. Graph showing MFI of lysozyme in different groups; n = 6.

(L) qPCR analysis of Notch-related genes (*Math1*, *Dll1*, *Dll4*, *Jag1*, and *Hes1*) in the ileum; n = 6.

Data represent the mean \pm SD of three independent experiments; comparisons performed with t tests (two groups) or ANOVA (multiple groups). *p < 0.05, **p < 0.01, ***p < 0.001.

signaling offers great potential for effective therapeutic approaches to promote intestinal health.

Limitations of the study

We showed that *B. subtilis* inhibited the proliferation of Lgr5⁺ ISCs but significantly promoted the differentiation toward the secretory cell line. However, due to the lack of lineage tracing experiments, other mechanisms independent of ISC function may be involved in the differentiation of intestinal secretory lineages by *B. subtilis*. Our current results suggest that MAMP-LTA from *B. subtilis* participates, at least in part, in the process of Notch signaling inhibition in a TLR2-MyD88-dependent manner. However, future studies are needed to further explore the mechanism of TLR2 regulation by *B. subtilis*.

STAR★METHODS

Detailed methods are provided in the online version of this paper and include the following:

- KEY RESOURCES TABLE
- RESOURCE AVAILABILITY
 - Lead contact
 - Materials availability
 - Data and code availability
- EXPERIMENTAL MODEL AND SUBJECT DETAILS
 - Mice
 - Bacterial strains and cell culture
- METHOD DETAILS
 - Mouse intestinal organoid isolation, culture, and passage
 - Establishment of bacteria and intestinal organoid co-cultures
 - Mouse model of *S. typhimurium* infection
 - *Salmonella* colonization of intestinal organoids
 - Plate counts
 - Amp bacteriostatic experiment *in vitro*
 - Immunofluorescence assay
 - Flow cytometry
 - Quantitative RT-PCR
 - Western blot
 - Cytokine detection
 - EdU staining
- QUANTIFICATION AND STATISTICAL ANALYSIS

SUPPLEMENTAL INFORMATION

Supplemental information can be found online at <https://doi.org/10.1016/j.celrep.2022.111416>.

ACKNOWLEDGMENTS

We acknowledge J.R. Turner for providing the method and suggestion of intestinal organoids culture. This study was supported by the National Key R&D Program of China (2018YFE0127300); the National Natural Science Foundation of China (31972631 and 32002261); the Natural Science Foundation of Jiangsu Province (no. BK20200536); the China Postdoctoral Science Foundation funded project (BX20190153); and a project funded by the Priority Academic Program Development of Jiangsu Higher Education Institutions (PAPD).

AUTHOR CONTRIBUTIONS

Q.H., J.J., J.L., L.Z., and S.X. were responsible for performing the cellular experiments, data analysis, and writing the manuscript. Q.H., J.J., and Y.L. were responsible for the animal experiments and data analysis. Q.Y. and Y.L. were responsible for the conception and design of the study, drafting the article, and final approval of the version submitted.

DECLARATION OF INTERESTS

The authors have no conflict of interest.

Received: June 12, 2021

Revised: August 17, 2022

Accepted: September 1, 2022

Published: September 27, 2022

REFERENCES

- Bevins, C.L., and Salzman, N.H. (2011). Paneth cells, antimicrobial peptides and maintenance of intestinal homeostasis. *Nat. Rev. Microbiol.* 9, 356–368.
- Birchenough, G.M.H., Johansson, M.E.V., Gustafsson, J.K., Bergström, J.H., and Hansson, G.C. (2015). New developments in goblet cell mucus secretion and function. *Mucosal Immunol.* 8, 712–719.
- Buck, S.B., Bradford, J., Gee, K.R., Agnew, B.J., Clarke, S.T., and Salic, A. (2008). Detection of S-phase cell cycle progression using 5-ethynyl-2'-deoxyuridine incorporation with click chemistry, an alternative to using 5-bromo-2'-deoxyuridine antibodies. *Biotechniques* 44, 927–929.
- Cheesman, S.E., Neal, J.T., Mittge, E., Sereidick, B.M., and Guillemin, K. (2011). Epithelial cell proliferation in the developing zebrafish intestine is regulated by the Wnt pathway and microbial signaling via Myd88. *Proc. Natl. Acad. Sci. USA* 108, 4570–4577.
- Clevers, H. (2013). The intestinal crypt, a prototype stem cell compartment. *Cell* 154, 274–284.
- Dutta, D., and Clevers, H. (2017). Organoid culture systems to study host-pathogen interactions. *Curr. Opin. Immunol.* 48, 15–22.
- Fre, S., Bardin, A., Robine, S., and Louvard, D. (2011). Notch signaling in intestinal homeostasis across species: the cases of *Drosophila*, Zebrafish and the mouse. *Exp. Cell Res.* 317, 2740–2747.
- Gazit, R., Krizhanovskiy, V., and Ben-Arie, N. (2004). Math1 controls cerebellar granule cell differentiation by regulating multiple components of the Notch signaling pathway. *Development* 131, 903–913.
- Gehart, H., and Clevers, H. (2019). Tales from the crypt: new insights into intestinal stem cells. *Nat. Rev. Gastroenterol. Hepatol.* 16, 19–34.
- Grabinger, T., Luks, L., Kostadinova, F., Zimmerlin, C., Medema, J.P., Leist, M., and Brunner, T. (2014). Ex vivo culture of intestinal crypt organoids as a model system for assessing cell death induction in intestinal epithelial cells and enteropathy. *Cell Death Dis.* 5, e1228.
- Hou, Q., Dong, Y., Huang, J., Liao, C., Lei, J., Wang, Y., Lai, Y., Bian, Y., He, Y., Sun, J., et al. (2020a). Exogenous L-arginine increases intestinal stem cell function through CD90+ stromal cells producing mTORC1-induced Wnt2b. *Commun. Biol.* 3, 611.
- Hou, Q., Huang, J., Ayansola, H., Masatoshi, H., and Zhang, B. (2020b). Intestinal stem cells and immune cell relationships: potential therapeutic targets for inflammatory bowel diseases. *Front. Immunol.* 11, 623691.
- Hou, Q., Ye, L., Huang, L., and Yu, Q. (2017). The research progress on intestinal stem cells and its relationship with intestinal microbiota. *Front. Immunol.* 8, 599.
- Hou, Q., Ye, L., Liu, H., Huang, L., Yang, Q., Turner, J.R., and Yu, Q. (2018). *Lactobacillus accelerates ISCs regeneration to protect the integrity of intestinal mucosa through activation of STAT3 signaling pathway induced by LPLs secretion of IL-22.* *Cell Death Differ.* 25, 1657–1670.
- In, J.G., Foulke-Abel, J., Estes, M.K., Zachos, N.C., Kovbasnjuk, O., and Donowitz, M. (2016). Human mini-guts: new insights into intestinal physiology

- and host-pathogen interactions. *Nat. Rev. Gastroenterol. Hepatol.* **13**, 633–642.
- Jensen, J., Pedersen, E.E., Galante, P., Hald, J., Heller, R.S., Ishibashi, M., Kageyama, R., Guillemot, F., Serup, P., and Madsen, O.D. (2000). Control of endodermal endocrine development by Hes-1. *Nat. Genet.* **24**, 36–44.
- Kazanjan, A., Noah, T., Brown, D., Burkart, J., and Shroyer, N.F. (2010). Atonal homolog 1 is required for growth and differentiation effects of Notch/gamma-secretase inhibitors on normal and cancerous intestinal epithelial cells. *Gastroenterology* **139**, 918–928.e1-6.
- Kim, J.J., and Khan, W.I. (2013). Goblet cells and mucins: role in innate defense in enteric infections. *Pathogens* **2**, 55–70.
- Kim, Y.S., and Ho, S.B. (2010). Intestinal goblet cells and mucins in health and disease: recent insights and progress. *Curr. Gastroenterol. Rep.* **12**, 319–330.
- Kretzschmar, K., and Clevers, H. (2016). Organoids: modeling development and the stem cell niche in a dish. *Dev. Cell* **38**, 590–600.
- Kundu, P., Blacher, E., Elinav, E., and Pettersson, S. (2017). Our gut microbiome: the evolving inner self. *Cell* **171**, 1481–1493.
- Lebeer, S., Vanderleyden, J., and De Keersmaecker, S.C.J. (2010). Host interactions of probiotic bacterial surface molecules: comparison with commensals and pathogens. *Nat. Rev. Microbiol.* **8**, 171–184.
- Lee, Y.S., Kim, T.Y., Kim, Y., Lee, S.H., Kim, S., Kang, S.W., Yang, J.Y., Baek, I.J., Sung, Y.H., Park, Y.Y., et al. (2018). Microbiota-derived lactate accelerates intestinal stem-cell-mediated epithelial development. *Cell Host Microbe* **24**, 833–846.e6.
- Lievín-Le Moal, V., and Servin, A.L. (2006). The front line of enteric host defense against unwelcome intrusion of harmful microorganisms: mucins, antimicrobial peptides, and microbiota. *Clin. Microbiol. Rev.* **19**, 315–337.
- Liu, H., Xu, W., Yu, Q., and Yang, Q. (2017). 4, 4'-diaponeurosporene-producing *Bacillus subtilis* increased mouse resistance against *Salmonella typhimurium* infection in a CD36-dependent manner. *Front. Immunol.* **8**, 483.
- Lu, X., Xie, S., Ye, L., Zhu, L., and Yu, Q. (2020). *Lactobacillus* protects against *S. Typhimurium*-induced intestinal inflammation by determining the fate of epithelial proliferation and differentiation. *Mol. Nutr. Food Res.* **64**, e1900655.
- Mahapatro, M., Foersch, S., Hefele, M., He, G.W., Giner-Ventura, E., McHedlidze, T., Kindermann, M., Vetrano, S., Danese, S., Günther, C., et al. (2016). Programming of intestinal epithelial differentiation by IL-33 derived from pericryptal fibroblasts in response to systemic infection. *Cell Rep.* **15**, 1743–1756.
- Mahe, M.M., Aihara, E., Schumacher, M.A., Zavros, Y., Montrose, M.H., Helmrath, M.A., Sato, T., and Shroyer, N.F. (2013). Establishment of gastrointestinal epithelial organoids. *Curr. Protoc. Mouse Biol.* **3**, 217–240.
- Ootani, A., Li, X., Sangiorgi, E., Ho, Q.T., Ueno, H., Toda, S., Sugihara, H., Fujimoto, K., Weissman, I.L., Capecchi, M.R., et al. (2009). Sustained in vitro intestinal epithelial culture within a Wnt-dependent stem cell niche. *Nat. Med.* **15**, 701–706.
- Palaga, T., Buranaruk, C., Rengpipat, S., Fauq, A.H., Golde, T.E., Kaufmann, S.H.E., and Osborne, B.A. (2008). Notch signaling is activated by TLR stimulation and regulates macrophage functions. *Eur. J. Immunol.* **38**, 174–183.
- Puschhof, J., Pleguezuelos-Manzano, C., and Clevers, H. (2021). Organoids and organs-on-chips: insights into human gut-microbe interactions. *Cell Host Microbe* **29**, 867–878.
- Sato, T., van Es, J.H., Snippert, H.J., Stange, D.E., Vries, R.G., van den Born, M., Barker, N., Shroyer, N.F., van de Wetering, M., and Clevers, H. (2011). Paneth cells constitute the niche for Lgr5 stem cells in intestinal crypts. *Nature* **469**, 415–418.
- Sato, T., Vries, R.G., Snippert, H.J., van de Wetering, M., Barker, N., Stange, D.E., van Es, J.H., Abo, A., Kujala, P., Peters, P.J., et al. (2009). Single Lgr5 stem cells build crypt-villus structures in vitro without a mesenchymal niche. *Nature* **459**, 262–265.
- Shang, Y., Smith, S., and Hu, X. (2016). Role of Notch signaling in regulating innate immunity and inflammation in health and disease. *Protein Cell* **7**, 159–174.
- Siebel, C., and Lendahl, U. (2017). Notch signaling in development, tissue homeostasis, and disease. *Physiol. Rev.* **97**, 1235–1294.
- Snippert, H.J., van der Flier, L.G., Sato, T., van Es, J.H., van den Born, M., Kroon-Veenboer, C., Barker, N., Klein, A.M., van Rheenen, J., Simons, B.D., et al. (2010). Intestinal crypt homeostasis results from neutral competition between symmetrically dividing Lgr5 stem cells. *Cell* **143**, 134–144.
- Troll, J.V., Hamilton, M.K., Abel, M.L., Ganz, J., Bates, J.M., Stephens, W.Z., Melancon, E., van der Vaart, M., Meijer, A.H., Distel, M., et al. (2018). Microbiota promote secretory cell determination in the intestinal epithelium by modulating host Notch signaling. *Development* **145**, dev155317.
- Tsai, Y.H., VanDussen, K.L., Sawey, E.T., Wade, A.W., Kasper, C., Rakshit, S., Bhatt, R.G., Stoeck, A., Maillard, I., Crawford, H.C., et al. (2014). ADAM10 regulates Notch function in intestinal stem cells of mice. *Gastroenterology* **147**, 822–834.e13.
- van der Flier, L.G., and Clevers, H. (2009). Stem cells, self-renewal, and differentiation in the intestinal epithelium. *Annu. Rev. Physiol.* **71**, 241–260.
- van der Flier, L.G., Haegebarth, A., Stange, D.E., van de Wetering, M., and Clevers, H. (2009). OLFM4 is a robust marker for stem cells in human intestine and marks a subset of colorectal cancer cells. *Gastroenterology* **137**, 15–17.
- van Es, J.H., de Geest, N., van de Born, M., Clevers, H., and Hassan, B.A. (2010). Intestinal stem cells lacking the Math1 tumour suppressor are refractory to Notch inhibitors. *Nat. Commun.* **1**, 18.
- van Es, J.H., van Gijn, M.E., Riccio, O., van den Born, M., Vooijs, M., Begthel, H., Cozijnsen, M., Robine, S., Winton, D.J., Radtke, F., et al. (2005). Notch/gamma-secretase inhibition turns proliferative cells in intestinal crypts and adenomas into goblet cells. *Nature* **435**, 959–963.
- Vogt, C.M., Hilbe, M., Ackermann, M., Aguilar, C., and Eichwald, C. (2018). Mouse intestinal microbiota reduction favors local intestinal immunity triggered by antigens displayed in *Bacillus subtilis* biofilm. *Microb. Cell Fact.* **17**, 187.
- Wu, H., Xie, S., Miao, J., Li, Y., Wang, Z., Wang, M., and Yu, Q. (2020). *Lactobacillus reuteri* maintains intestinal epithelial regeneration and repairs damaged intestinal mucosa. *Gut Microb.* **11**, 997–1014.
- Wu, H., Ye, L., Lu, X., Xie, S., Yang, Q., and Yu, Q. (2018). *Lactobacillus acidophilus* alleviated *Salmonella*-induced goblet cells loss and colitis by Notch pathway. *Mol. Nutr. Food Res.* **62**, e1800552.
- Yamamoto, S., and Harayama, S. (1995). PCR amplification and direct Sequencing of *gyrB* genes with universal primers and their application to the detection and taxonomic analysis of *Pseudomonas putida* strains. *Appl. Environ. Microbiol.* **61**, 3768.
- Yang, Q., Bermingham, N.A., Finegold, M.J., and Zoghbi, H.Y. (2001). Requirement of Math1 for secretory cell lineage commitment in the mouse intestine. *Science* **294**, 2155–2158.
- Zhang, Q., Wang, C., Liu, Z., Liu, X., Han, C., Cao, X., and Li, N. (2012). Notch signal suppresses Toll-like receptor-triggered inflammatory responses in macrophages by inhibiting extracellular signal-regulated kinase 1/2-mediated nuclear factor kappaB activation. *J. Biol. Chem.* **287**, 6208–6217.
- Zhang, Y.G., Wu, S., Xia, Y., and Sun, J. (2014). *Salmonella*-infected crypt-derived intestinal organoid culture system for host-bacterial interactions. *Physiol. Rep.* **2**, e12147.

STAR★METHODS

KEY RESOURCES TABLE

REAGENT or RESOURCE	SOURCE	IDENTIFIER
Antibodies		
Goat anti-mouse DyLight 488	Abcam	Cat#: ab150117; RRID:AB_2688012
Goat anti-rabbit DyLight 594	Abcam	Cat#: ab150080; RRID:AB_2650602
Goat anti-rabbit DyLight 488	WellBio technology	Cat#: WB0193
Rabbit polyclonal anti-DCLK1	Abcam	Cat#: ab37994; RRID:AB_873538
Rabbit polyclonal anti-Hes1	Abcam	Cat#: ab71559; RRID:AB_1209570
Mouse monoclonal anti-Lysozyme	Abcam	Cat#: ab36362; RRID:AB_776115
Rabbit monoclonal anti-Muc2	HUABIO	Cat#: ET1704-06
Mouse monoclonal anti-Math1	Abcam	Cat#: ab27667; RRID:AB_870587
Rabbit polyclonal anti-NICD1	Abcam	Cat#: ab8925; RRID:AB_306863
Anti- <i>E. coli</i> lipopolysaccharide (LPS)	Abcam	Cat#: ab35654; RRID:AB_732222
Rabbit polyclonal anti-MyD88	Abcam	Cat#: ab2064; RRID:AB_302807
APC anti-mouse CD24 antibody [M1/69]	BioLegend	Cat#: 101840; RRID: AB_2650876
Rabbit polyclonal anti-Ki67	Bioss	Cat#: bs-23101R
Rabbit monoclonal anti-Olfm4	Cell Signaling Technology	Cat#: 39141; RRID:AB_2650511
Anti-lipoteichoic acid (LTA)	Invitrogen	Cat#: MA1-40134; AB_1076514
Goat anti-mouse IgG(H+L) HRP	MultiSciences Biotech	Cat#: 70-GAM0072
Goat anti-rabbit IgG(H+L) HRP	ZCIBIO Technology	Cat#: ZC-G2106
IgG2a-APC	MultiSciences Biotech	Cat#: 70-CRG2a05-10
Mouse polyclonal anti-DLL4	R&D systems	Cat#: AF1389; RRID:AB_354770
Mouse polyclonal anti-TLR2	R&D systems	Cat#: AF1530; RRID:AB_354847
Mouse monoclonal anti-Alpi	Santa Cruz	Cat#: sc-271431; RRID:AB_10649489
Mouse monoclonal anti- β -tubulin	Sangon Biotech	Cat#: D410006
Rabbit polyclonal anti-GAPDH	Zen-bio	Cat#: 380626
Bacterial and virus strains		
<i>Bacillus subtilis</i> 168	(Liu et al., 2017)	Available from the Liu lab
<i>Bacillus subtilis</i> WB800	(Liu et al., 2017)	Available from the Liu lab
<i>Salmonella typhimurium</i> SL1344	(Liu et al., 2017)	Available from the Liu lab
<i>Lactobacillus acidophilus</i>	ATCC	ATCC 4356
<i>E. coli</i> O157	ATCC	ATCC BAA-1883
Chemicals, peptides, and recombinant proteins		
Recombinant mouse DLL4 protein	Abcam	Cat#: ab208307
TLR2 inhibitor CUCPT22	Absin	Cat#: abs814483
Mouse TNF- α ELISA kit	BlueGene	Cat#: E03T0008
Mouse TNF- α ELISA kit	NeoBioscience	Cat#: EMC102a.48
Mouse Defa1 ELISA kit	Jiangsu Meimian Industrial	Cat#: MM-45791M1
Mouse Defa5 ELISA kit	Jiangsu Meimian Industrial	Cat#: MM-44728M1
Mouse Ang4 ELISA kit	Jiangsu Meimian Industrial	Cat#: MM-0212M1
Mouse PLA2G2A ELISA kit	Jiangsu Meimian Industrial	Cat#: MM-45802M1
Mouse TFF3 ELISA kit	Jiangsu Meimian Industrial	Cat#: MM-45277M1
Mouse IL-1 β ELISA kit	Shanghai Lian Shuo Biotechnology	Cat#: AE90731Mu
LPS assay kit	J&L Biological	Cat#: JL20691
ECL Substrate Kit	HAKATA	Cat#: H-E-60
γ -secretase inhibitor DAPT	MOLNOVA	Cat#: M13243

(Continued on next page)

Continued		
REAGENT or RESOURCE	SOURCE	IDENTIFIER
Recombinant mouse TFF3 protein	Novoprotein	Cat#: C661
Cell-Light EdU DNA cell proliferation kit	Guangzhou RiboBio	Cat#: C10310-2
Recombinant JAG-1 protein	R&D Systems	Cat#: MAB599
Recombinant Ang4 protein	R&D Systems	Cat#: 964-AN-025
lipoteichoic acid (LTA) from <i>Bacillus subtilis</i>	Sigma-Aldrich	Cat#: L3265
FITC-UEA-1	Sigma-Aldrich	Cat#: L9006
4',6-Diamidino-2-Phenylindole (DAPI)	Invitrogen	Cat#: D1306
IntestiCult™ Organoid Growth Medium (Mouse)	STEMCELL	Cat#: 06000
Fetal bovine serum	VivaCell	Cat#: C04001
Recombinant mouse Noggin protein	PeproTech	Cat#: 250-38
Recombinant mouse R-spondin1 protein	PeproTech	Cat#: 315-32
Recombinant Rat EGF protein	T&L Biological Technology	Cat#: GMP-TL676
Experimental models: Cell lines		
Human epithelial colorectal adenocarcinoma	Chuanqiu Biotechnology	Cat#: H010
Experimental models: Organisms/strains		
mouse: C57BL/6J	Yangzhou University	Animal Research Centre
mouse: <i>Smoc-Tlr2^{em1Smoc}</i> : C57BL/6J	Nanjing University	Nanjing Biomedical Research Institute
mouse: <i>Lgr5^{tm1(cre/ERT2)Cle}</i> : C57BL/6J	(Hou et al., 2020a)	Available from the Hou lab
Oligonucleotides		
RT-qPCR primers	This paper	Table S1
Software and algorithms		
FlowJo	Tree Star	https://www.flowjo.com
Prism	Graphpad	https://www.graphpad.com/scientific-software/prism/
ImageJ	National Institutes of Health	https://imagej.nih.gov/ij/

RESOURCE AVAILABILITY

Lead contact

Further information and requests for resources and reagents should be directed to and will be fulfilled by the lead contact, Yuchen Li (yuchengli@njau.edu.cn).

Materials availability

This study did not generate new unique reagents.

Data and code availability

This paper does not report original code. All data reported in this paper will be shared by the [lead contact](#) upon request. Any additional information required to reanalyze the data reported in this paper is available from the [lead contact](#) upon request.

EXPERIMENTAL MODEL AND SUBJECT DETAILS

Mice

All mice were bred in-house and maintained on a C57BL/6J background. C57BL/6J mice (specific-pathogen-free [SPF]) were purchased from the Animal Research Centre of Yangzhou University. TLR2^{-/-} C57BL/6J mice (SPF) were purchased from the Nanjing Biomedical Research Institute of Nanjing University. Lgr5-EGFP-IRES-CreERT2 (Lgr5-GFP) mice (SPF) were purchased from Jackson Laboratory. Male mice were aged 4-12 weeks, and were age-matched for independent experiments. The exact number of animals used per experiment is indicated in the figure legends. All animal studies were approved by the Institutional Animal Care and Use Committee (IACUC) of Nanjing Agricultural University (NJAU.No20211213195).

Bacterial strains and cell culture

Bacillus subtilis, *E. coli*, and *S. typhimurium* SL1344 were grown in Luria-Bertani (LB) broth (10 g tryptone, 5 g yeast extract, and 5 g NaCl per L) or on LB plates (Life-iLab, Shanghai, AN61L516) fortified with 1.5% agar at 37°C. *Lactobacillus acidophilus* was grown in

deMan, Rogosa, and Sharpe (MRS) medium at 37°C. *Salmonella typhimurium* SL1344 is streptomycin-resistant. High-pressure steam sterilization was used to kill *B. subtilis* (121°C/20 psi for 20 min). All the strains will be dispersed and counted by Ultrasonic Bacteria Dispersion Counter (SCIENTZ-CF) before use. Human epithelial colorectal adenocarcinoma (Caco-2) cells (Shanghai Chuanqiu Biotechnology) were grown in complete medium (Dulbecco's modified Eagle medium (DMEM), 10% fetal bovine serum (FBS) (VivaCell, Shanghai), 2 mM L-glutamine, and 1% non-essential amino acids). Cells were digested in Trypsin (Hangzhou Putai Biotechnology Co., LTD) and seeded in 24-well plates at a density of 1.5×10^5 cells/well and incubated for 2 d, reaching full confluence at 37°C with 5% CO₂.

METHOD DETAILS

Mouse intestinal organoid isolation, culture, and passage

As previously described (Sato et al., 2009), ileal and colonic organoids were obtained from respective tissues of four-week-old C57BL/6 mice in an independent experiment. The experiment was repeated three times, and each time the organoids were isolated and pooled from three different mice. Briefly, the ileum and colon were removed immediately after euthanizing the mice with CO₂. Organs were opened longitudinally, washed with sterile PBS, and cut into pieces. Small intestinal pieces were incubated in small intestinal crypt isolation buffer (2 mM ethylenediaminetetraacetic acid [EDTA] in Dulbecco's phosphate buffered saline [DPBS]) for 30 min at 4°C on a rocking platform. Colon pieces were incubated in colonic crypt isolation buffer (5.6 mM Na₂HPO₄, 8 mM KH₂PO₄, 9.8 mM NaCl, 1.6 mM KCl, 44 mM Sucrose, 24.8 mM D-sorbitol, 5 mM EDTA, and 0.5 mM DL-dithiothreitol in distilled water). The mixture was passed through a 70-μm cell strainer (Jet Biofil), and small intestinal and colonic crypt fractions were isolated and purified by centrifugation. Matrigel (Corning) was added to a pellet of crypt fractions, and 50 μL drops of crypt-containing Matrigel were added to the wells of a 24-well plate. For small intestinal organoid culture, advanced DMEM/F12 (Gibco) supplemented with 100 U/mL penicillin, 0.1 mg/mL streptomycin (Solarbio), 10 mM HEPES (Gibco), N-2 (Gibco), B-27 (Gibco), 50 ng/mL mouse epidermal growth factor (EGF) (Beijing T&L Biological Technology Co., Ltd.), 100 ng/mL mouse Noggin (Peprotech), and 500 ng/mL mouse R-spondin1 (Peprotech) was added. For colonic organoid culture, IntestiCult™ Organoid Growth Medium (STEMCELL) supplemented with 100 U/mL penicillin and 0.1 mg/mL streptomycin (Solarbio) was added. The culture medium and growth factors were replaced every 3–4 d.

For organoid passage, the tissue culture plate was placed on ice to thaw the Matrigel, and the medium was aspirated. A 1 mL volume of cold PBS was added to each well. The mixture was pipetted up and down to disperse, centrifuged for 4 min at 300 × g and 4°C, and decanted to remove PBS. The remaining pellet was resuspended in 50 μL of Matrigel/well and allowed to polymerize. Each well was then overlaid with 650 μL of the culture medium.

Establishment of bacteria and intestinal organoid co-cultures

Co-culture systems containing different bacteria and intestinal organoids were constructed according to the pattern diagram in Figure S1A. Briefly, organoids were harvested in cold PBS and washed once to remove Matrigel. To obtain organoid buds, organoids were vigorously pipetted through a 1 mL syringe to induce mechanical disruption. After shearing, the buds were washed once in advanced DMEM/F12 (Gibco) and then incubated with live *B. subtilis* 168/HK *B. subtilis* 168/*B. subtilis* WB800/*Lactobacillus acidophilus* ATCC4356/*E. coli* in 1 mL culture medium (100 buds per 1×10^4 CFU of bacteria). After 2 h of co-incubation in a 37°C shaker, buds were washed once with culture medium to remove unbound bacteria. Organoid buds were then re-embedded into 50 μL Matrigel in 24-well tissue culture plates (400 buds/well; Jet Biofil) and incubated in 500 μL culture medium at 37°C with 5% CO₂ for 3–7 d. 1% Penicillin-streptomycin was used to inhibit bacterial growth in the medium. In some experiments, the organoids were treated with the γ-secretase inhibitor DAPT (Molnova, M13243), the Notch ligand DLL4 (5 μg/mL, ab208307), lipoteichoic acid (LTA) from *Bacillus subtilis* (30 μg/mL, Sigma, L3265), and/or TLR2 inhibitor CUCPT22 (10 μM, Absin, abs814483). Samples were harvested at the indicated time points. To address the differential capacities of the strains to attach to organoids, organoid lysates were plated on LB agar plates and cultured at 37°C for 16 h. Then, the number of bacterial colonies on the plates was counted. The organoids were incubated overnight with primary antibodies (anti-lipoteichoic acid (LTA), 1:50, Invitrogen™, MA1-40134; anti-*E. coli* lipopolysaccharide (LPS), 1:50, Abcam, ab35654). The samples were incubated with DyLight 488 (1:200, Abcam, ab150117)-conjugated secondary antibodies for 1 h, followed by 4',6-Diamidino-2-Phenylindole (DAPI) (1:5,000, Invitrogen™, D1306) for 5 min at 25°C. The median fluorescence intensity (MFI) of LTA was analyzed using ImageJ software.

Mouse model of *S. typhimurium* infection

Male C57BL/6J (WT, eight weeks old) mice were orally administered *B. subtilis* 168 (1×10^8 CFU) or PBS as a control once a day for 21 days. In the *Salmonella* test, each mice was orally administered *S. typhimurium* strain 1344 (1×10^8 CFU) once on day 14. All mice were weighed daily and euthanized with CO₂ on day 21. The intestinal tissues were removed immediately and the length of the intestine was measured. Ascending sections from the ileum of each mouse were analyzed using a hematoxylin and eosin (HE) staining kit (Beijing Leagene Biotechnology Co., Ltd., Beijing, China) and a PAS staining kit (Beijing Leagene Biotechnology).

Salmonella colonization of intestinal organoids

Salmonella colonization of intestinal organoids was largely performed according to a published procedure (Zhang et al., 2014). Briefly, intestinal organoids were harvested in cold PBS and washed once to remove Matrigel. To obtain organoid buds, organoids were vigorously pipetted through a 1 mL syringe. After shearing, buds were washed once in advanced DMEM/F12 (Gibco) and then incubated with *S. typhimurium* SL1344 in 1 mL culture medium (100 buds per 1×10^4 CFU bacteria). After 30 min co-incubation in a 37°C shaker, cultures were rinsed twice with culture medium to remove unbound bacteria. The buds were re-embedded into 50 μ L Matrigel in 24-well tissue culture plates (400 buds per well; NEST Biotechnology) at 37°C with 5% CO₂. After 2 h, 500 μ L culture medium containing gentamicin (500 μ g/mL) was added to each well to kill extracellular *S. typhimurium*. Samples were collected for western blotting, ELISA, and real-time PCR after the intestinal organoids were colonized with *Salmonella* for 12 h. Disrupted organoids were defined by the absence of a defined edge; the presence of disordered, diffuse cells; a lack of obvious structural elements; and a dark central region (Grabinger et al., 2014).

Salmonella was stained with BacLight™ Bacterial Green Stain (B-35000, Molecular Probes) according to manufacturer instructions. Briefly, 10^7 CFU of *Salmonella* and 100 μ M working solution of the BacLight bacterial stain were dissolved in DMSO and incubated for 15 min at 25°C. The *Salmonella* samples were washed with PBS to remove excess dye. To visualize *Salmonella* invasion into the organoids, we used a fluorescence-labeled strain of *Salmonella* to colonize the cultures for 90 min. The samples were examined using a Zeiss 710 laser scanning confocal microscope.

Plate counts

Intestinal organoids were treated with *B. subtilis*, DLL4, and *S. typhimurium* according to the detailed methods described in Figure 5B. Briefly, intestinal organoids were first treated with or without *B. subtilis* and DLL4 for three days. They were incubated with 1% penicillin-streptomycin at the indicated times to inhibit the growth of *B. subtilis*. After 3 d, extracellular *B. subtilis* was washed away with HBSS containing 3% penicillin-streptomycin. The intestinal organoids were then infected with the indicated *Salmonella* strains for 30 min, washed with HBSS, and incubated in mini-gut media containing gentamicin (500 mg/mL) for the indicated times. After 12 h, the intestinal organoids were dissociated using TrypLE. After the mixtures were vigorously pipetted through a p200 pipette to induce mechanical disruption, single cells were washed twice with PBS. Then, 2 mL of sterile water was mixed with 1×10^6 cells per tube for lysis. The homogenates were centrifuged at $600 \times g$ for 10 min, and the supernatants were plated on LB agar plates containing 500 μ g/mL streptomycin and cultured at 37°C for 16 h. The number of resulting bacterial colonies on each plate was counted. *B. subtilis* detection by plate counting in the intestine was largely performed according to previous study (Vogt et al., 2018). First, most microorganisms in ileal contents were killed by Pasteurization (80°C for 20 minutes). Then *B. subtilis* spores in remaining contents were resuscitated in LB medium in a 37°C shaker for 2 hours. Then the CFU number of *B. subtilis* was detected by plate counting.

Amp bacteriostatic experiment in vitro

Two methods were used to verify bacteriostatic Amps experiments *in vitro*: 1) Caco-2 cells were incubated with Ang4, lysozyme, and Defa5 for 12 h. Cells were washed once with PBS and then cultured in complete medium (0.5 mL containing 5×10^5 CFU *S. typhimurium* SL1344 per well). After 1 h of co-incubation, cells were washed three times with PBS to remove unbound bacteria and cultured with complete medium for 12 h. 2) Caco-2 cells were cultured with 0.5 mL complete medium containing 5×10^5 CFU *S. typhimurium* SL1344 per well. After 1 h of co-incubation, the cells were washed three times with PBS to remove unbound bacteria and cultured in complete medium containing Ang4, lysozyme, and Defa5 for 12 h. After treatment with the above two methods, single cells were harvested using TrypLE and washed twice with PBS containing 5% FBS. Then, 1 mL of sterile water was mixed with 1×10^5 cells per tube for lysis. The homogenates were centrifuged at $600 \times g$ for 10 min, and the supernatants were plated on LB agar plates containing 500 μ g/mL streptomycin and cultured at 37°C for 16 h. Then, the number of bacterial colonies on the plates was counted.

Immunofluorescence assay

The intestinal organoids used in the different groups were rinsed three times in ice-cold HBSS and then suspended in cold HBSS. The intestinal organoids were spun down at $300 \times g$ for 10 min at 4°C, then fixed overnight in 4% paraformaldehyde. Sections of the ileum (2 cm each) were collected from mice in different groups, fixed overnight in 4% paraformaldehyde, embedded in optimal cutting temperature compound, cut into 8 μ m thick slices, and rinsed in HBSS. The intestinal organoids and tissue sections were permeabilized with 0.5% Triton X-100 for 20 min, washed three times with HBSS, and incubated for 1 h in 5% bovine serum albumin in HBSS to reduce nonspecific background signals. For IF staining, intestinal organoids and tissue sections were incubated overnight with primary antibodies (anti-Hes1, 1:50, Abcam, ab71559; anti-Math1, 1:50, Abcam, ab27667; anti-NICD1, 1:50, Abcam, ab8925; anti-Lysozyme, 1:50, Abcam, ab36362; anti-DCLK1, 1:50, ab37994; anti-Olfm4, 1:50, CST, 39141; anti-Muc2, 1:50, HUABIO, ET1704-06; anti-Alpi, 1:50, Santa Cruz, sc-271431; anti-Ki67, 1:50; Bioss, bs-23101R). The samples were then incubated with goat anti-mouse DyLight 488 (1:200, Abcam, ab150117), goat anti-rabbit DyLight 488 (1:200, WellBio technology, WB0193), and goat anti-rabbit DyLight 594 (1:200, Abcam, ab150080)-conjugated secondary antibodies for 1 h, followed by DAPI (1:5,000, Invitrogen™, D1306) for 5 min at 25°C. Secretory cells in the intestinal organoids and ilea were fixed with 4% paraformaldehyde and then stained with UEA-1 (1:200, Sigma, L9006) for 1 h at 25°C. The samples were examined using a Zeiss 710 laser scanning

confocal microscope. Fluorescence images were collected for further qualitative and quantitative analyses. Goblet cells in the ileal segments of mice treated or not treated with *B. subtilis* were stained with PAS. The numbers of UEA-1⁺, lysozyme⁺ and of Muc2⁺, DCLK1⁺, and PAS⁺ cells per villus and crypt were counted manually. The MFI of Hes1, NICD1, and Lgr5 was analyzed using ImageJ software.

Flow cytometry

ISCs and Paneth cells were isolated from Lgr5-GFP mice using a modified crypt isolation protocol with 20 min of 2.5 mM EDTA followed by several strainer steps and 5 min incubation with TrypLE and 0.8 kU/mL of DNase1 under minute-to-minute vortexing to form a single-cell suspension. This suspension was incubated for 30 min on ice in 1 mL of culture medium containing an antibody cocktail of CD24-APC (BioLegend, M1/69, 1:500) or IgG2a-APC isotype control (MultiSciences, 70-CRG2a05-10). The samples were filtered through 40 μ m mesh (NEST Biotechnology) before cell sorting. ISCs were isolated as Lgr5^{hi}, and Paneth cells were isolated as CD24+SSC^{hi} with a BD FACS Aria II SORP cell sorter into the supplemented crypt culture medium. Isolated ISCs were centrifuged at 250 \times g for 5 min, resuspended in an appropriate volume of crypt culture medium, and seeded onto 50 mL Matrigel (Corning) containing 1 mM JAG-1 protein (R&D Systems) in 24-well plates. For Lgr5⁺ ISC culture, IntestiCultTM Organoid Growth Medium (STEMCELL) supplemented with 100 U/mL penicillin and 0.1 mg/mL streptomycin (Solarbio) was added. The culture medium was replaced every 3–4 d. According to published procedure (Sato et al., 2011), we used flow cytometry to analyze the populations of Lgr5-GFP^{hi} (Lgr5⁺ ISC) and Lgr5-GFP^{low} (progenitor) cells from the organoids derived from Lgr5⁺ ISCs. The organoids were incubated in TrypLE Express (Gibco) under minute-to-minute vortexing to form a single-cell suspension. GFP⁺ analysis gates were established such that Lgr5-GFP^{hi} events were detectable in intestinal organoids from Lgr5-GFP mice.

Quantitative RT-PCR

Total RNA from intestinal tissues, contents, and organoids was extracted using an automated nucleic acid extractor (Scientz-NP-2032). *Gyrase subunit B* (*gyrB*) was used to detect *Bacillus subtilis* in the intestine (Yamamoto and Harayama, 1995). Two microliters of template RNA was reacted with SYBR PCR Master Mix for a final volume of 20 μ L (Genstar). Reagents were added to 96-well PCR plates (LABLEAD Inc). The thermal cycling conditions were: 5 min at 95°C, followed by 40 cycles of 15 s at 95°C and 34 s at 60°C, using an Applied Biosystems 7500 real-time PCR system. See Table S1 for primer information.

Western blot

The intestinal organoids from different groups were rinsed three times in ice-cold HBSS, suspended in ice-cold HBSS, and then spun down at 300 \times g for 10 min at 4°C. Next, a pipette was used to aspirate the PBS at the top, and the organoids were lysed in RIPA buffer containing a protease inhibitor cocktail (Thermo Fisher Scientific). Protein concentrations were determined using a BCA Protein Quantification Kit (Thermo Fisher). Equal amounts of protein were separated by SDS-PAGE and electrophoretically transferred onto polyvinylidene fluoride membranes (Millipore, China). After the membranes were blocked in 5% nonfat milk in TBS containing 0.1% Tween-20, they were probed with anti-Hes1 (Abcam, 1:1000; ab71559), anti-Math1 (Abcam, 1:1000; ab27667), anti-DLL4 (R&D systems, 1:1,000, AF1389), anti-TLR2 (R&D systems, 1:1,000, AF1530), and anti-MyD88 (Abcam, 1:1000; ab2064) antibodies. Anti- β -tubulin (Sangon Biotech, 1:1000; D410006) and anti-GAPDH (Zen-bio, 1:1000; 380626) antibodies were used for normalization. The membranes were washed and then incubated with goat anti-rabbit secondary antibody (Shanghai zcbio technology Co., Ltd., 1:5,000; ZC-G2106) and goat anti-mouse secondary antibody (MultiSciences, 1:5,000; 70-GAM0072). Signals were detected using a ECL Substrate Kit (HAKATA; H-E-60/125/250) and analyzed using an Image Reader LAS-4000 imaging system (Fujifilm, Tokyo, Japan).

Cytokine detection

Organoid culture media were obtained, and IL-1 β (Shanghai Lian Shuo Biotechnology Co., Ltd., AE90731Mu) and TNF- α (BlueGene, E03T0008; NeoBioscience, EMC102a.48) levels were measured using ELISA kits according to manufacturer instructions. Ileal tissues (1 cm) and organoids were harvested and homogenized in PBS (0.5 mL) with 1 mM PMSF. Samples were then centrifuged for 10 min at 12000 \times g, and total protein in the supernatant was quantified using a PierceTM BCA Protein Assay Kit (Solarbio, PC0020). Supernatant (0.5 mg protein in 0.1 mL) was assayed for cytokines using mouse Defa1 (MM-45791M1), Defa5 (MM-44728M1), Ang4 (MM-0212M1), PLA2G2A (MM-45802M1), and TFF3 (MM-45277M1) ELISA kits (all purchased from Jiangsu Meimian Industrial Co., Ltd.) according to manufacturer instructions. The LPS concentration in the serum was measured using an LPS assay kit (Jianglai, China, JL20691) according to manufacturer instructions.

EdU staining

Cell proliferation in intestinal organoids that were or were not treated with *B. subtilis* was assessed using a Cell-Light EdU DNA cell proliferation kit (RiboBio; C103102) according to manufacturer instructions. Briefly, intestinal organoids were exposed to 25 mM EdU (RiboBio) for 2 h at 37°C and then fixed in 4% paraformaldehyde. After permeabilization with 0.5% Triton X-100, the cells were incubated with a 1 \times Apollo reaction cocktail (RiboBio) for 30 min. Subsequently, the cells were stained with Hoechst 33342 for 30 min to analyze DNA content, then visualized under a Zeiss 710 laser-scanning confocal microscope or a Nuohai LS18 light sheet microscopy (Nuohai Life Science (Shanghai) Co., Ltd). The MFI of EdU was analyzed using ImageJ software.

QUANTIFICATION AND STATISTICAL ANALYSIS

All details on number of subjects and samples can be found in the [results](#) section/figure legends. The results were expressed as mean \pm SD from at least three independent experiments, unless otherwise stated. One-way analysis of variance was employed to identify significant differences among multiple groups, and the *t*-test was employed to identify significant differences between two groups; **p* < 0.05, ***p* < 0.01, ****p* < 0.001.

Cell Reports, Volume 40

Supplemental information

***Bacillus subtilis* programs the differentiation
of intestinal secretory lineages
to inhibit *Salmonella* infection**

Qihang Hou, Junpeng Jia, Jian Lin, Linda Zhu, Shuang Xie, Qinghua Yu, and Yuchen Li

Supplementary information

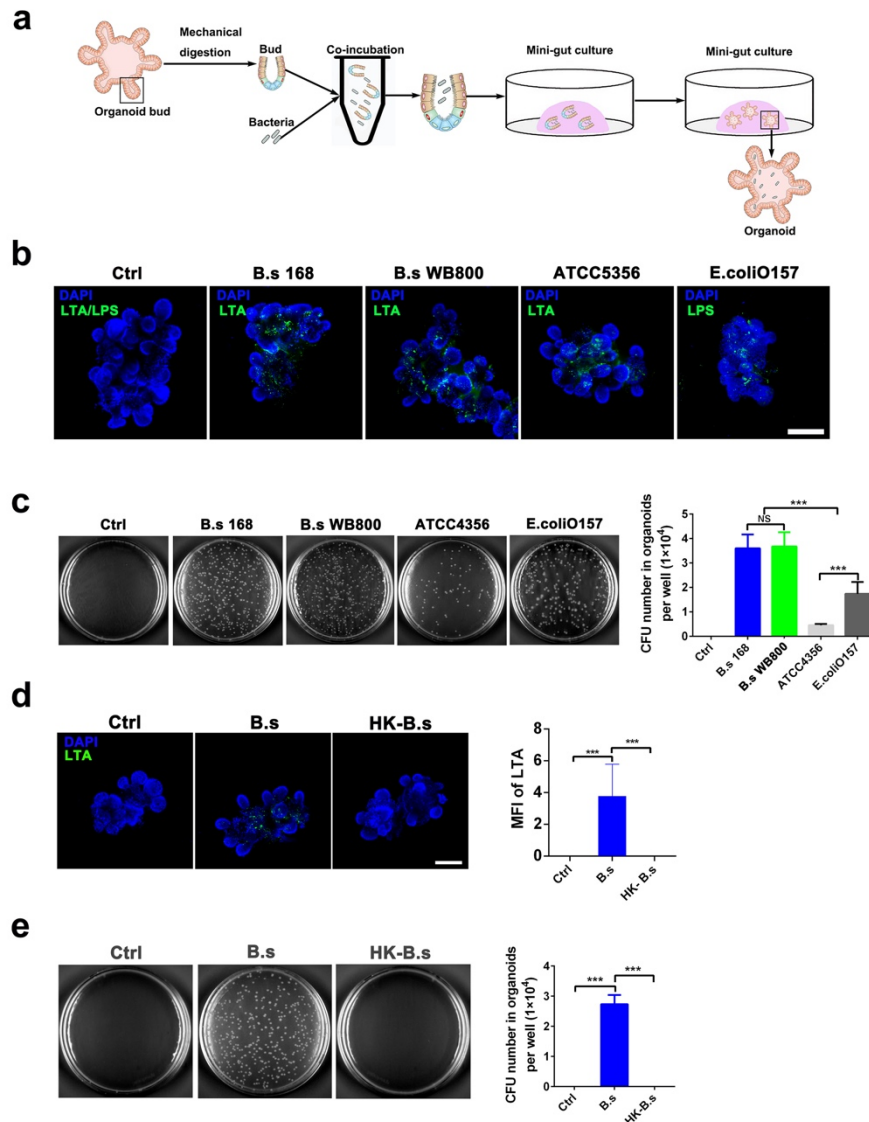


Figure S1. Building a co-cultured system with bacteria and intestinal organoids, related to Figure 1 (a) Pattern diagram of constructing the co-culture model of vDAPI (blue) in small intestinal organoids. Scale bar, 100 μm . (b) Immunostaining of EdU (Red), LTA/LPS (green), and DAPI (blue) in small intestinal organoids. Scale bar, 100 μm . (c) CFU count of different bacteria in the organoids per well; $n = 6$. (d) Immunostaining of EdU (Red), LTA (green), and DAPI (blue) in the organoids. Scale bar, 100 μm . Graph showing MFI of LTA; $n = 6$ organoids per group. (e) CFU count of *B. subtilis* 168 in the organoids per well; $n = 6$. Data represent the mean \pm SD of two or three independent experiments; comparisons performed with analysis of variance (ANOVA) (multiple groups). * $P < 0.05$, ** $P < 0.01$, *** $P < 0.001$.

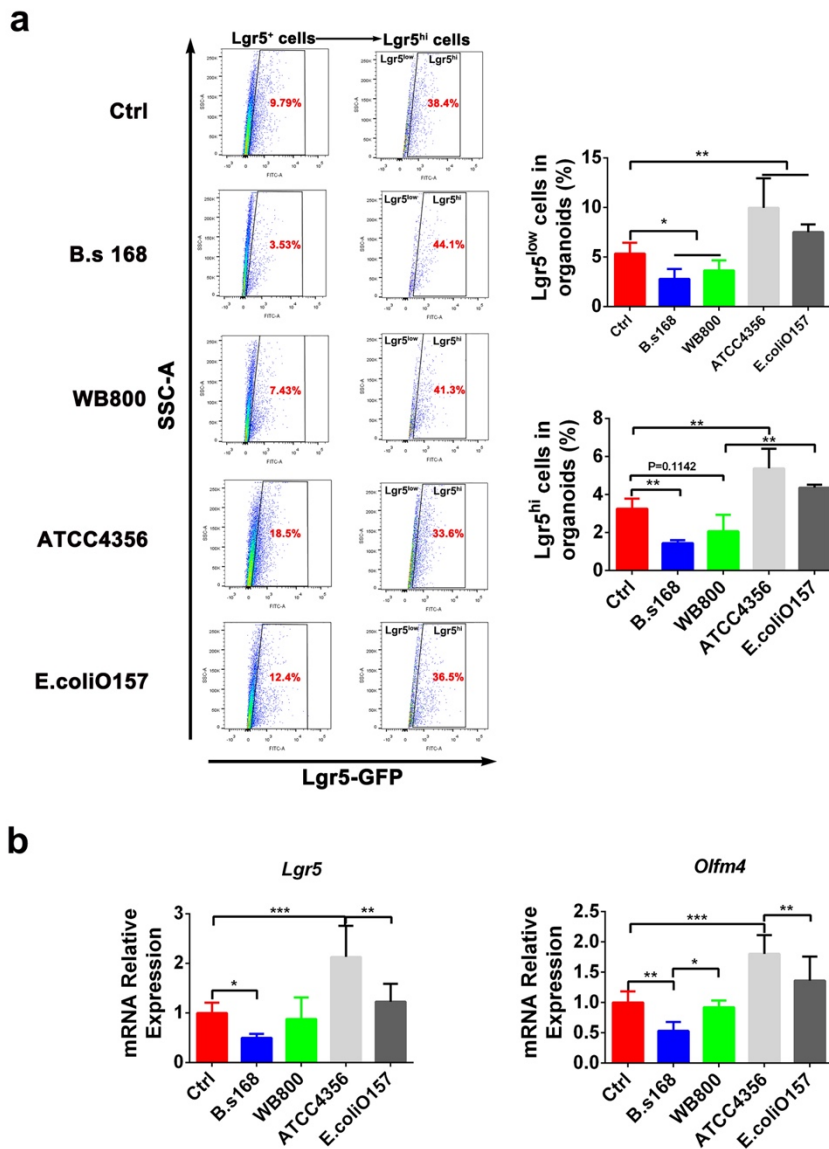


Figure S2. Effect of different bacterial treatments on Lgr5⁺ ISC pool, related to Figure 1 (a) Flow cytometry analysis of Lgr5-GFP^{low} and Lgr5-GFP^{hi} ISC frequencies in small intestinal organoids from different groups; n = 3. (b) qPCR analysis of Lgr5⁺ ISC marker genes (*Lgr5* and *Olfm4*) in small intestinal organoids; n = 6. Data represent the mean ± SD of two or three independent experiments; comparisons performed with analysis of variance (ANOVA) (multiple groups). **P* < 0.05, ***P* < 0.01, ****P* < 0.001.

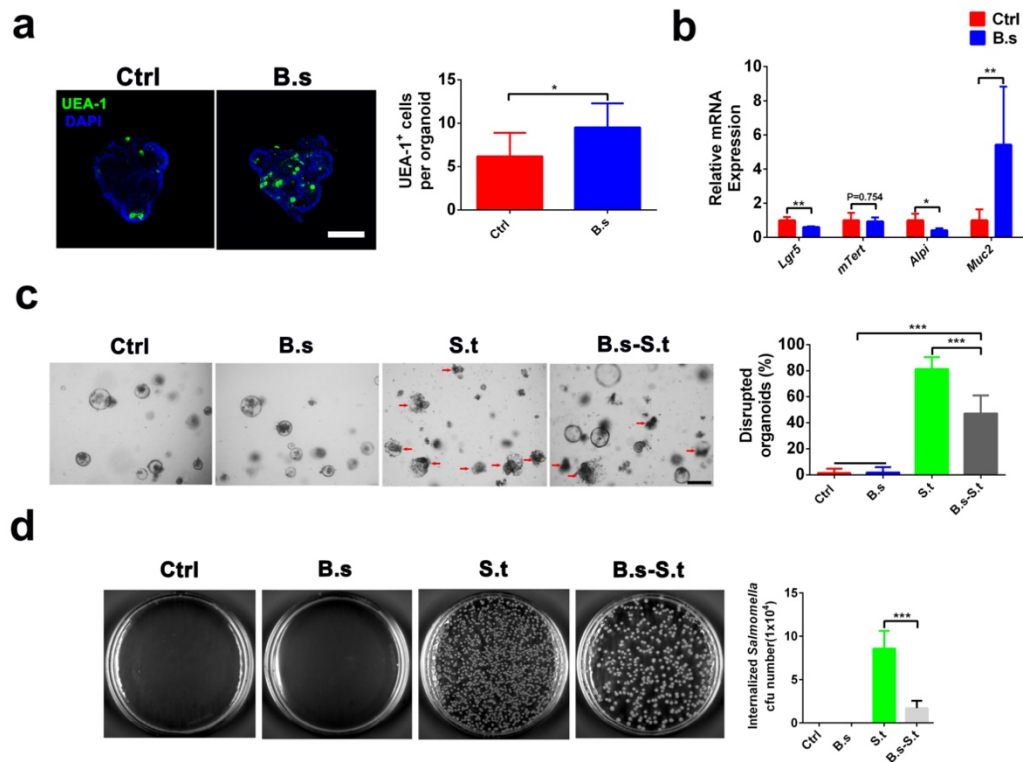


Figure S3. *Bacillus subtilis* modulates the differentiation of secretory lineage cells and provides protection against the pathogen *Salmonella typhimurium* in colonic organoids, related to Figure 1 and 6 (a) Immunostaining of UEA-1 (green) and DAPI (blue) in colonic organoids. Scale bar, 100 μ m. Graph showing UEA-1⁺ cells per organoid bud; n = 12 organoids per group. (b) qPCR for markers of intestinal epithelial cell types in colonic organoids: Lgr5⁺ ISCs (*Lgr5*), +4 ISCs (*mTert*), absorptive enterocytes (*Alpi*), and goblet cells (*Muc2*); n = 6. (c) Relative number of disrupted colonic organoids (red arrow) at 12 h post-infection: n = 6. (d) Number of invasive *Salmonella* cells in colonic organoids obtained from different groups at 12 h post-infection; n = 6. Data represent the mean \pm SD of two or three independent experiments; comparisons performed with *t*-tests (two groups) or analysis of variance (ANOVA) (multiple groups). **P* < 0.05, ***P* < 0.01, ****P* < 0.001.

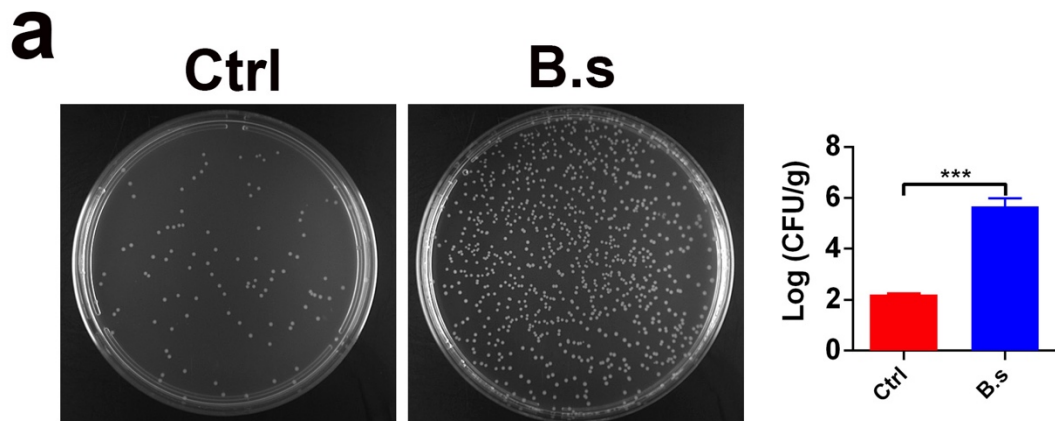


Figure S4. CFU count of *B. subtilis* in ileal contents, related to Figure 3 (a) CFU count of *B. subtilis* in ileal contents was determined by plate counting; $n = 6$. Data represent the mean \pm SD of two or three independent experiments; comparisons performed with *t*-tests (two groups). * $P < 0.05$, ** $P < 0.01$, *** $P < 0.001$.

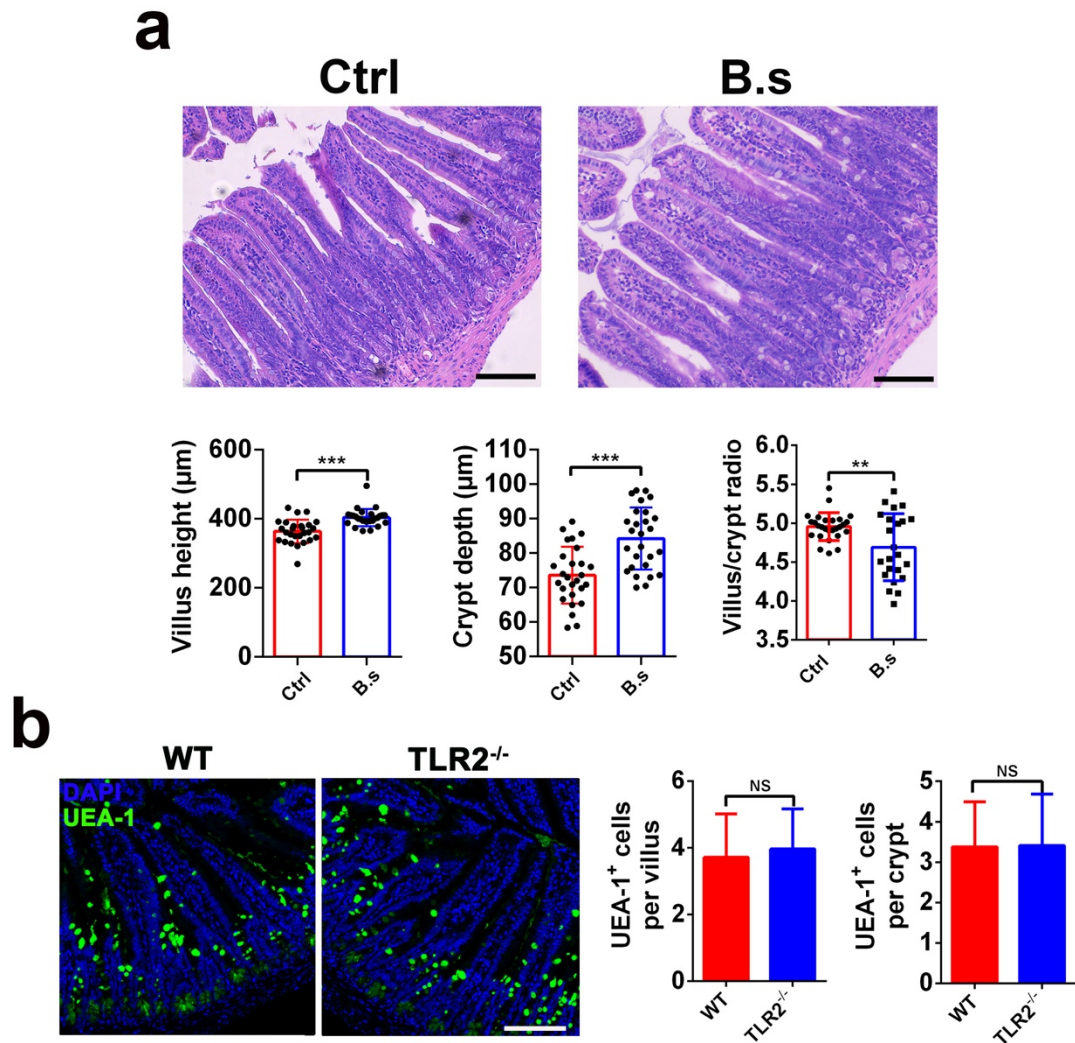


Figure S5. Intestinal morphology and number of secretory cells, related to Figure 4

a) Representative pictures of the HE staining in the ileum. Scale bar, 100 μm . Graph showing villus height, crypt depth, and villus/crypt ratio; $n = 6$ mice per group. **(b)** Immunostaining of UEA-1 (green) and DAPI (blue) in the ileum of WT or TLR2^{-/-} mice. Scale bar, 100 μm . Graph showing UEA-1⁺ cell per villus and crypt; $n = 6$. Data represent the mean \pm SD of two or three independent experiments; comparisons performed with *t*-tests (two groups). * $P < 0.05$, ** $P < 0.01$, *** $P < 0.001$.

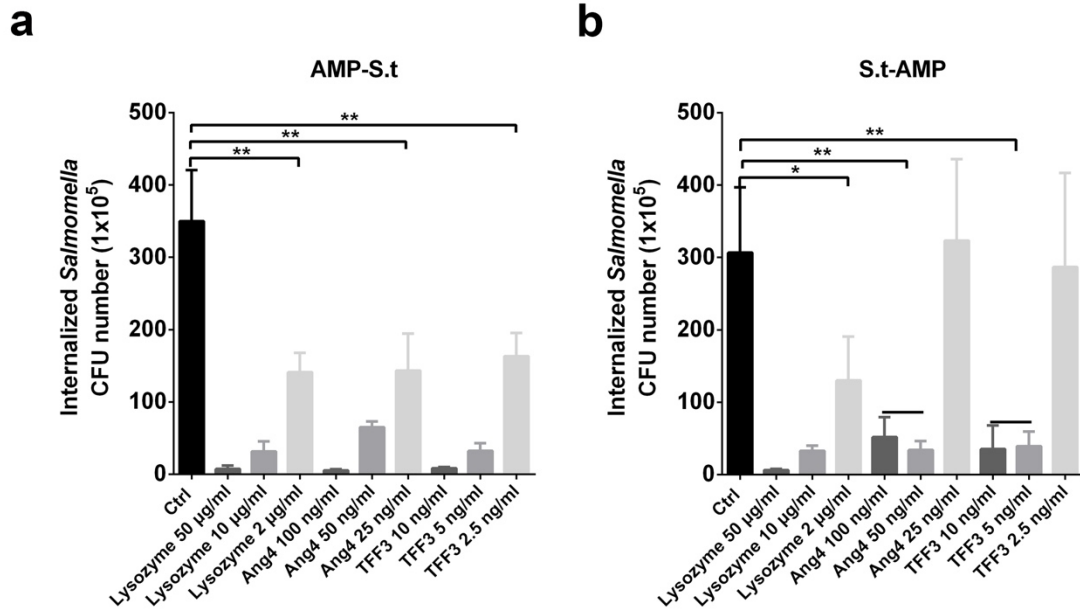


Figure S6. AMPs limit the invasion of *S. typhimurium* into Caco-2 cells, related to Figure 5 and 6 (a) Number of invasive *Salmonella* cells in AMP pre-treated Caco2 cells at 12 h post-infection; n = 3. (b) Number of invasive *Salmonella* in Caco2 cells co-incubated with APMS at 12 h post-infection; n = 3. Data represent the mean \pm SD of two or three independent experiments; comparisons performed with analysis of variance (ANOVA) (multiple groups). * $P < 0.05$, ** $P < 0.01$, *** $P < 0.001$.

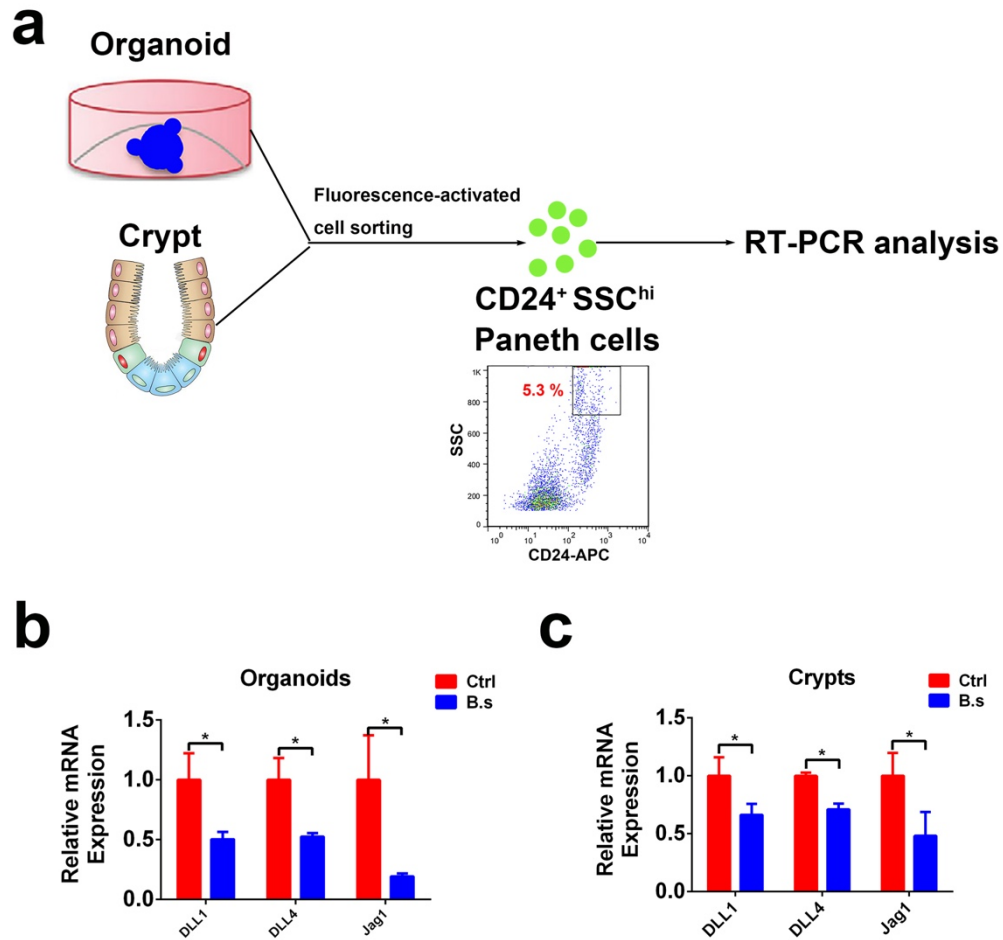


Figure S7. Expression of Notch ligands in Paneth cells, related to Figure 2 and 7
(a) Experimental flow chart. **(b)** qPCR analysis of the Notch ligand genes *Dll1*, *Dll4*, and *Jag-1* in Paneth cells isolated from intestinal organoids; n = 4. **(c)** qPCR analysis of *Dll1*, *Dll4*, and *Jag-1* in Paneth cells isolated from ileal crypts; n = 4. Data represent the mean \pm SD of three independent experiments; comparisons performed with *t*-tests (two groups). * $P < 0.05$, ** $P < 0.01$, *** $P < 0.001$.

Table S1 Primer sequences used for qRT-PCR. Related to STAR Methods

Mouse	Forward	Reverse	Product size (bp)
Lyz1	GAGACCGAAGCACCGACTATG	CGGTTTTGACATTGTGTTCGC	214
Muc2	CAATGACAAGGTGTCCCTGCC	GTGCTCTCCAAACTCTCTGG	889
ChgA	ATCCTCTCTATCCTGCGACAC	GGGCTCTGGTTCTCAAACACT	158
Alpi	GGGACCTCCATCTTTGGTCTG	AACTCTGAGCTTCGGTGAC	134
Sox9	CGGAACAGACTCACATCTCTCC	GCTTGCACGTCGGTTTTGG	163
Klf4	GTGCCCCGACTAACCGTTG	GTCGTTGAACTCCTCGGTCT	185
Defa1	GCTGCCTGCTCATCCTAATC	CAGCATCAGTGGCCTCAGTA	376
Ang4	GGTTGTGATTCTCCAACTCTG	CTGAAGTTTTCTCCATAAGGGT	228
Defa5	TTGGGCTCCTGCTCAACAAT	GACACAGCCTGGTCCTCTTC	168
PLA2G2A	CTATGCCTTCTATGGATGCCAC	CAGCCGTTTCTGACAGGAGT	205
Dll1	CAGGACCTTCTTTTCGCGTATG	AAGGGGAATCGGATGGGGTT	168
Dll4	TTCCAGGCAACCTTCTCCGA	ACTGCCGCTATTCTTGTCCTC	102
Hes1	CCAGCCAGTGTC AACACGA	AATGCCGGGAGCTATCTTTCT	166
TLR2	CAGCTTAAAGGGCGGGTCAGAG	TGGAGACGCCAGCTCTGGCTCA	380
MyD88	CCTGCGGTTTCATCACTAT	GGCTCCGCATCAGTCT	144
GADPH	ATGGTGAAGGTCGGTGTGAA	TGGAAGATGGTGATGGGCTT	227
Math1	CCCGTCAAAGTACGGGAACA	TGGAAGATGGTGATGGGCTT	166
TFF3	TTGCTGGGTCCTCTGGGATAG	ATCTGGGCCATCTGTAGGGT	257
Jag1	GCCTCAAAGAAGCGATCAGAA	GCACGACTGGAAAACAACACT	108
Notch1	GATCGACAACCGGCAATGTG	GGGCTTGAGGAATATTGAGGCT	116
Notch2	GGACCATCTTTTCGGAGGCA	GCGAGAATGTCTGGGCGATA	237
Lgr5	CGTCCCCTTCTTCTCTGTC	TATGCTGGCGTGGGTAAAGG	205
Olfm4	CTGCTATACACAGGTTTCAGGAGC	GTGCATGACAGAAAGGACGCT	116
mTert	TCTACCGCACTTTGGTTGCC	CAGCACGTTTCTCTCGTTGC	155
gyrB	CGGTCGTAAACGCACTATC	AGGGTCCGGGACAAAATGTGTCTG	158